AIP | The Journal of Chemical Physics

Density functional theory simulations of amorphous high-κ oxides on a compound semiconductor alloy: a-Al2O3/InGaAs(100)-(4×2), a-HfO2/InGaAs(100)-(4×2), and a-ZrO2/InGaAs(100)-(4×2)

Evgueni A. Chagarov and Andrew C. Kummel

Citation: The Journal of Chemical Physics **135**, 244705 (2011); doi: 10.1063/1.3657439
View online: http://dx.doi.org/10.1063/1.3657439
View Table of Contents: http://scitation.aip.org/content/aip/journal/jcp/135/24?ver=pdfcov
Published by the AIP Publishing

Density functional theory simulations of amorphous high-κ oxides on a compound semiconductor alloy: a-Al_2O_3/InGaAs(100)-(4×2), a-HfO_2/InGaAs(100)-(4×2), and a-ZrO_2/InGaAs(100)-(4×2)

Evgueni A. Chagarov and Andrew C. Kummel
Department of Chemistry and Biochemistry, University of California, San Diego, California 92093, USA

(Received 29 June 2011; accepted 11 October 2011; published online 27 December 2011)

The structural properties of a-Al_2O_3/$In_{0.5}Ga_{0.5}As$, a-HfO_2/$In_{0.5}Ga_{0.5}As$, and a-ZrO_2/$In_{0.5}Ga_{0.5}As$ interfaces were investigated by density-functional theory (DFT) molecular dynamics (MD) simulations. Realistic amorphous a-Al_2O_3, a-HfO_2, and a-ZrO_2 samples were generated using a hybrid classical-DFT MD "melt-and-quench" approach and tested against the experimental properties. For each stack type, two systems with different initial oxide cuts at the interfaces were investigated. All stacks were free of midgap states, but some had band-edge states which decreased the bandgaps by 0%–40%. The band-edge states were mainly produced by deformation, intermixing, and bond-breaking, thereby creating improperly bonded semiconductor atoms. The interfaces were dominated by metal-As and O−In/Ga bonds which passivated the clean surface dangling bonds. The valence band-edge states were mainly localized at improperly bonded As atoms, while conduction band-edge states were mainly localized at improperly bonded In and Ga atoms. The DFT-MD simulations show that electronically passive interfaces can be formed between high-κ oxides dielectrics and InGaAs if the processing does not induce defects because on a short time scale the interface spontaneously forms electrically passive bonds as opposed to bonds with midgap states. © *2011 American Institute of Physics*. [doi:10.1063/1.3657439]

I. INTRODUCTION

The rapid scaling of complementary metal oxide semiconductor (CMOS) technology requires substituting the traditional gate oxide, SiO_2, with high-κ dielectrics, which can maintain the same capacitance with much lower leakage current. Amorphous alumina (a-Al_2O_3), hafnia (a-HfO_2), and zirconia (a-ZrO_2) are major candidates for such high-κ gate oxide materials. InGaAs offers significantly higher mobility than silicon and is being extensively investigated for n-channel high-κ MOSFETs.[1–3]

Although there are previously reported density-functional theory (DFT) simulations of high-κ oxide-semiconductor interfaces, there are only few reports on amorphous oxide bonding; furthermore, most of these reports include simulation with an oxide stack which contains a SiO_2 interlayer, so the simulated interfaces lack direct amorphous high-κ oxide-semiconductor bonds.[4–8] Amorphous oxide-semiconductor interfaces are likely to be superior to crystalline oxide-semiconductor interfaces because they do not have oxide-substrate lattice mismatch leading to a high density of defects. Despite their chemical composition similarity to the corresponding crystalline phase materials, amorphous Al_2O_3, HfO_2, and ZrO_2 demonstrate quite different microstructure, coordination distribution, and atomic chemical environment. Whereas some previously reported simulations of oxide-semiconductor interfaces were limited to artificially formed structures relaxed at 0 K, included crystalline oxides, and employed a bulk terminated binary semiconductors such as GaAs,[9–12] this study employs highly realistic amorphous high-κ oxide samples, a reconstructed ternary semiconductor surface (InGaAs), and uses full-scale DFT molecular dynamics (DFT-MD) at finite temperature, thereby providing the system with enough freedom to naturally evolve into the more realistic states.

The paper is organized as follows: Section I is an introduction (see above). Section II (which is mainly presented in the supplementary material) provides detailed descriptions of the amorphous sample generation, the computational techniques, and the stack annealing procedure. Section III encompasses the main results: (a) interfacial bonding, (b) InGaAs deformation, (c) Bader charge analysis, (d) coordination analysis, and (e) electronic structure analysis. Section IV presents the detailed comparison to experimental data. Section V presents the comparison to DFT crystalline oxide/GaAs models. Section VI presents a final conclusion.

II. GENERATION OF AMORPHOUS a-Al_2O_3, a-ZrO_2, AND a-HfO_2 SAMPLES: COMPUTATIONAL DETAILS OF THE OXIDE/InGaAs STACK FORMATION

The realistic amorphous a-Al_2O_3, a-ZrO_2, and a-HfO_2 samples perfectly matching the $In_{0.5}Ga_{0.5}As$(4×2)-(100) substrate surface area were generated by hybrid classical–DFT MD "melt and quench" approach.[13–16] For details of amorphous sample generation and oxide/InGaAs DFT-MD annealing, see supplementary material[16] and Refs. 17–49.

[a]Electronic mail: echagarov@ucsd.edu.

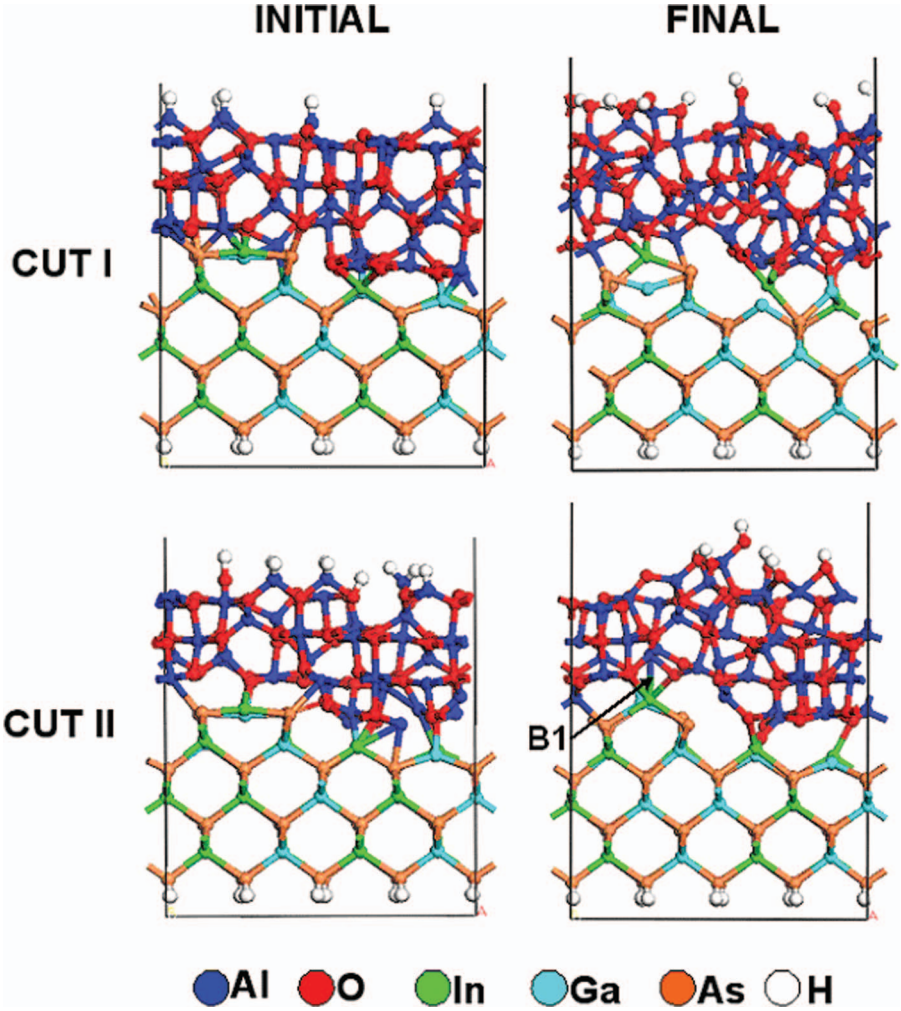

FIG. 1. Initial and final configurations of a-Al_2O_3/InGaAs interfaces (cut I and cut II). Although initially there are combinations of all bonds, the final configuration is dominated by Al−As and O−In/Ga bonds. As an exception, the a-Al_2O_3/InGaAs (cut II) system demonstrated single Al−In bond for sixfold coordinated In (bond "B1"), which did not create band-edge states.

III. RESULTS AND DISCUSSION

A. Bonding structure

The a-Al_2O_3/$In_{0.5}Ga_{0.5}As$(100)-(4×2) interfaces were annealed at 800 K, cooled and relaxed in two modifications (cut I and cut II) having different oxide cuts in initial systems (Fig. 1). Although the initial system had a mixture of Al−As, Al−Ga/In, O−As, and O−Ga/In bonds, after 1 ps annealing, cooling, and relaxation, the two systems evolved into final interface bonding structures formed by polar As−Al and In/Ga−O bonds neither with O−As bonds nor any intermixing via oxide metal atoms migration. As an exception, the a-Al_2O_3/InGaAs (cut II) system demonstrated single Al−In bond for sixfold coordinated In (bond "B1," Fig. 1), which did not create band-edge states probably because the Al−In bond was weak and long since the In was sixfold coordinated. The stacking of oxide to the InGaAs had significant impact on InGaAs surface reconstruction. For the a-Al_2O_3/InGaAs (cut I and cut II) stacks, half of InGaAs trough dimers were preserved, while the others were lost after stacking. While bonding to the oxide increased the coordination of most semiconductor surface atoms to fourfold, the semiconductor surface atoms which remained twofold and threefold coordinated strongly affected the electronic structure as discussed below. Some of the undercoordinated As atoms created valence band-edge states, while some broken III-As bonds contributed to conduction band-edge states. The high-temperature (1100 K) annealing of a-Al_2O_3/$In_{0.5}Ga_{0.5}As$ (cut I) interface resulted in complete interface delamination indicating generally weak oxide-semiconductor interfacial bonding.

The a-HfO_2/InGaAs (cut I and cut II) interfaces are presented in Fig. 2. Although the initial system had a mixture of Hf–As, Hf–Ga/In, O–As, and O–Ga/In bonds, within 1 ps, interfacial bonding both for cut I and cut II is formed by O−In/Ga and Hf−As bonds. In addition, the a-HfO_2/InGaAs (cut II) interface has a pair of As−O bonds, which do not produce band-edge or pinning states (bonds "B1,2," Fig. 2). The main difference between the cut I and cut II systems is a degree of interfacial intermixing. While the a-HfO_2/InGaAs (cut II) system demonstrates no intermixing, the a-HfO_2/InGaAs (cut I) interface reveals moderate intermixing with one Hf atom (atom "A1" in Fig. 2) migrated to the row-trough edge line and one In atom (atom "A2" in Fig. 2) pulled from

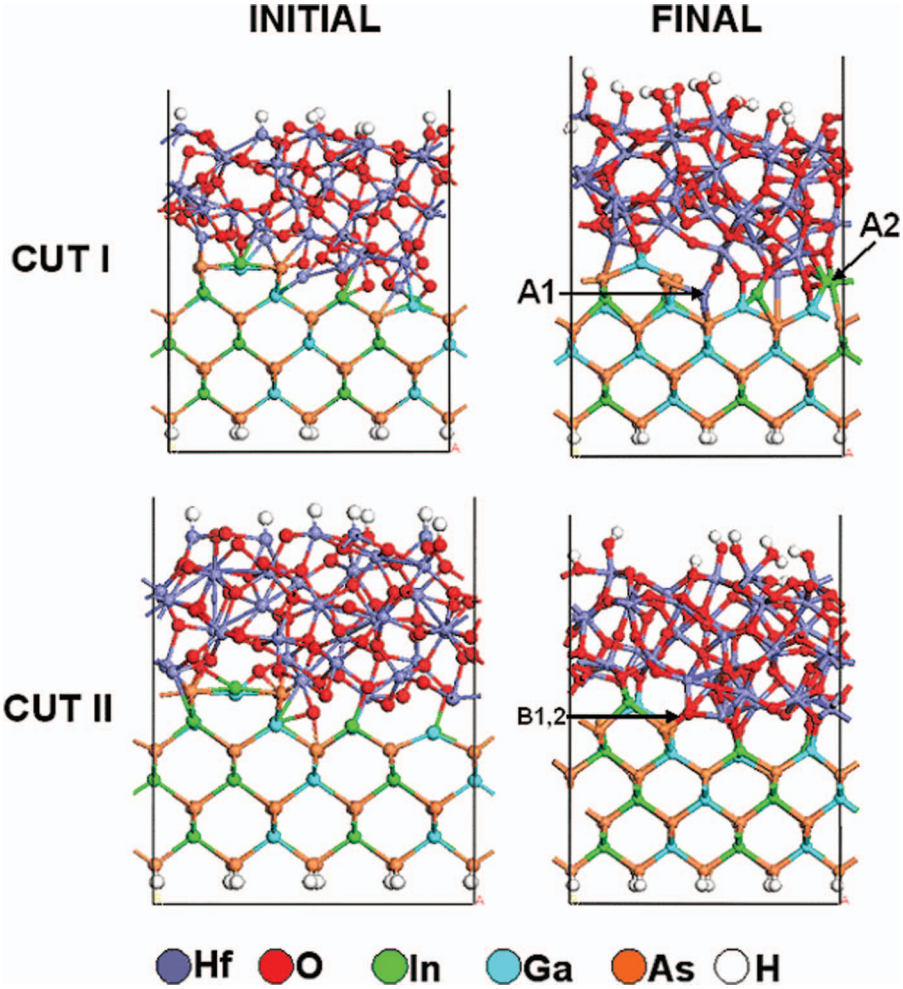

FIG. 2. Initial and final configurations of a-HfO_2/InGaAs interfaces (cut I and cut II). Although the initial system had a mixture of Hf−As, Hf-Ga/In, O−As, and O−Ga/In bonds, within 1 ps, the two systems evolved into final interface bonding structures formed mostly by As−Hf and In/Ga−O bonds with occasional O−As bonds. The cut I interface has one Hf atom (atom "A1") pulled towards the substrate and one In atom (atom "A2") pulled towards the oxide while retaining bonds to the substrate. The cut II interface has a pair of As−O bonds (bonds "B1,2").

InGaAs row dimer and migrated to InGaAs trough region. This migrated Hf atom contributes to both valence and conduction band-edge states, while As atom forming a bond to this Hf atom creates valence band-edge states, which will be discussed later in detail. For both interfaces, all InGaAs trough dimers were preserved after oxide stacking; however, for the cut I stack, one dimer was broken while later forming a similar dimer through periodic-boundary condition reflection.

Although the initial a-ZrO_2/InGaAs (cut I and cut II) interfaces (Fig. 3) had a mixture of Zr−As, Zr−Ga/In, O−As, and O−Ga/In bonds, within 1 ps of annealing, cooling, and relaxation the two systems evolved into final interface bonding structures formed by polar As−Zr and In/Ga−O bonds. For a-ZrO_2/InGaAs (cut I) interface, one In atom ("A1," Fig. 3) and one As atom ("A2," Fig. 3) from the InGaAs row region were pulled into the oxide with the In atom retaining one bond and the As retaining no bonds to the substrate. In the trough region, one Ga atom ("A3," Fig. 3) was pulled into the oxide retaining two bonds to the substrate atoms. For the cut I interface, half of the InGaAs trough dimers were preserved, while the other half were lost after stacking to the oxide. The a-ZrO_2/InGaAs (cut II) system demonstrated similar moderate deformation in InGaAs row region, where one In atom ("A4," Fig. 3), one Ga atom ("A5," Fig. 3), and two As atoms ("A6,""A7," Fig. 3) were pulled from the substrate towards the oxide while retaining bonds to InGaAs. In general, both a-ZrO_2/InGaAs interfaces demonstrated a O−In/Ga and Zr−As bonding pattern. As an exception, cut II interface had a single Zr−Ga bond with fivefold coordinated Ga ("B1," Fig. 3), which did not produce band-edge or pinning states. As discussed below, some of undercoordinated As atoms produce predominantly valence band-edge states, while some of undercoordinated In/Ga atoms create conduction band-edge states, which will be discussed later. The cut II interface preserves both InGaAs trough dimers after stacking to the oxide. The surface area of the DFT simulated InGaAs substrate is $\sim 16.94 \times 8.47$ Å^2; therefore, even several substrate atoms being pulled into the oxide indicate the potential for intermixing in the absence of surface passivation. The phenomenon of interface intermixing and substrate deformation will be quantified later in detail.

The initial InGaAs surface reconstruction has a mild effect on the final bonding geometry, while row-trough step-like topography has a larger (but moderate) effect on the final

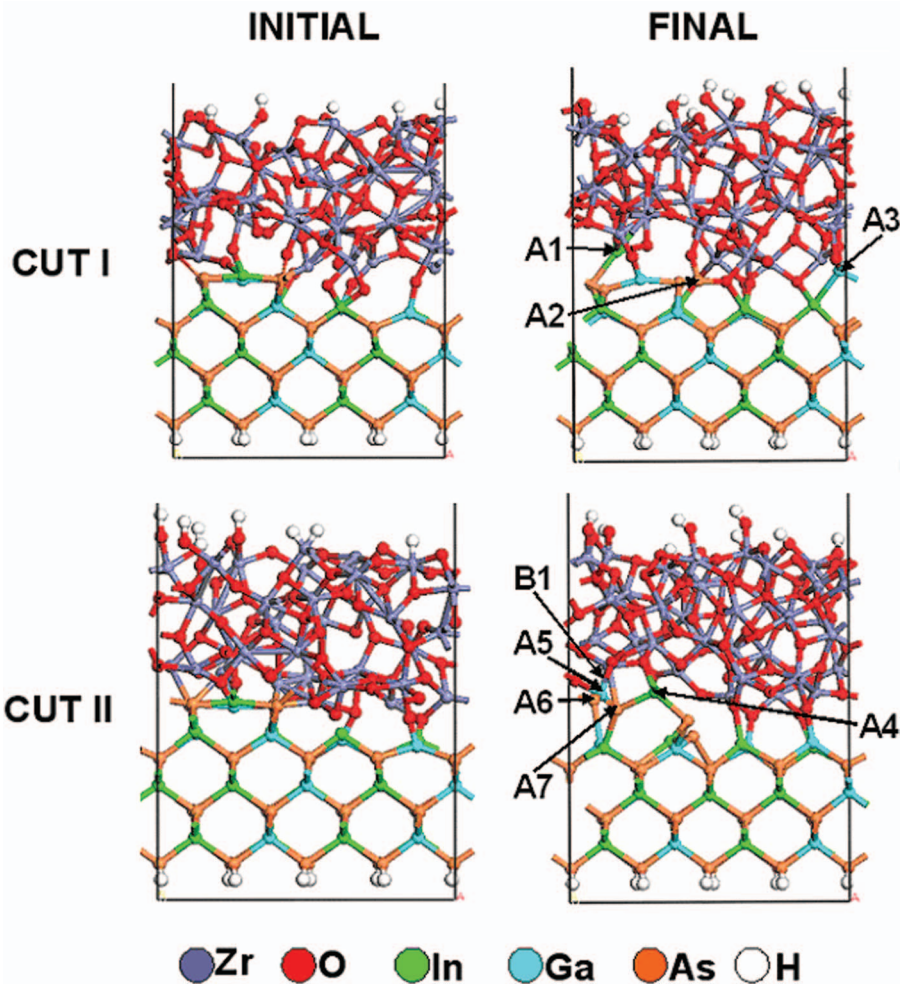

FIG. 3. Initial and final configurations of a-ZrO_2/InGaAs interfaces (cut I and cut II). Although initially there are combinations of all bonds, the final configuration is dominated by Zr−As and O−In/Ga bonds. The cut I interface has one row In atom ("A1"), one row As atom ("A2"), and one trough Ga atom ("A3) pulled into the oxide while retaining bonds to the substrate. The cut II interface has one row In atom ("A4"), one row Ga atom ("A5"), and two rows As atoms ("A6," "A7") pulled towards the oxide while retaining bonds to the substrate. The cut II interface has a single Zr−Ga bond with fivefold coordinated Ga ("B1").

oxide/semiconductor bonding. DFT-MD is a very accurate but computationally expensive technique, which limits simulated time scale. For real macroscopic processing which lasts for minutes, the effect of initial InGaAs reconstruction will be even weaker. While the exact details of the atomic structure of the 4×2 group III-rich reconstruction employed in this study probably have little influence on the final bonding geometry, it is noted that an As-rich reconstruction (typically 2×4) can also be prepared. Reconstructions with different ratios of group III to group V atoms on the surface are likely to strongly influence both atomic layer deposition (ALD) precursor chemistry and the bonding of the amorphous oxide to group V atoms on long time scales.[50]

B. Substrate deformation

The oxide-semiconductor interface intermixing and substrate deformation can significantly deteriorate the interfacial physical and electrical properties by decreasing carrier mobility, creating band-edge or midgap states pinning the interface, and forming an interfacial layer. The layer-by-layer substrate deformation in the annealed-cooled-relaxed oxide/semiconductor stack was quantified using the following norm:

$$\Delta \bar{R}_i = \frac{1}{N_i} \sum_j \left| \bar{R}_j - \bar{R}_{0j} \right|,$$

where N_i is the number of atoms in horizontal layer i, $\bar{R}_j$ and $\bar{R}_{0j}$ are the coordinates of atom j belonging to the horizontal layer i after the interface relaxation and in the initial relaxed InGaAs(4×2)-(100) clean substrate slab, while index j went along every substrate atom in horizontal layer i. The average layer-by-layer deformation of the InGaAs slab for all six cases is summarized in Fig. 4. The InGaAs slab has seven layers, which are counted from the bottom (layer 1) and up to the layer 7, which corresponds to the topmost InGaAs row region. The three bottom layers have zero deviation since they are fixed in space.

The a-Al_2O_3/InGaAs interfaces have no significant intermixing for both cuts (Fig. 1). There are only small displacements of InGaAs interface atoms and small InGaAs lattice distortions relative to the initial atomic positions in the clean InGaAs(4×2)-(100) substrate (Fig. 1). For the a-Al_2O_3/InGaAs models (Fig. 1), the average deviations per layer were 0.09 Å, 0.22 Å, 0.60 Å, and 0.59 Å for cut I, and

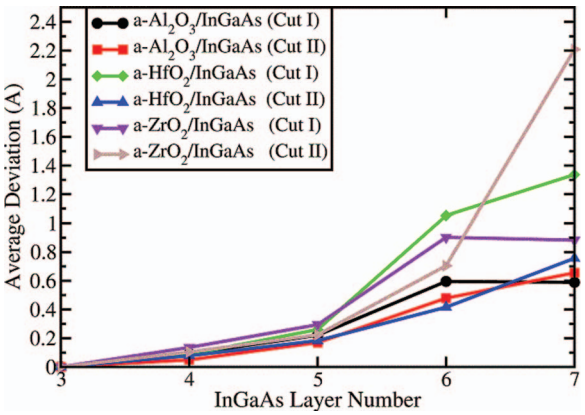

FIG. 4. Average layer-by-layer deformation of InGaAs slab for the investigated stacks. Note the a-Al_2O_3 (cut I and cut II) and the a-HfO_2 (cut II) stacks have the lowest deformation, while the a-HfO_2 (cut I) and a-ZrO_2 (cut I and cut II) stacks have the highest deformation due to intermixing.

0.05 Å, 0.17 Å, 0.48 Å, and 0.66 Å for cut II starting with the layer 4 in the bulk and moving up to the InGaAs surface (Fig. 4).

The a-HfO_2/InGaAs stacks (cuts I and II) demonstrated enhanced InGaAs layer displacements, especially for cut I. The average per-layer deviations of layers 6 and 7 for cut I system (1.05 Å and 1.34 Å) were significantly larger than for the cut II stack (0.42 Å and 0.76 Å) (Fig. 2), because in the a-HfO_2/InGaAs (cut I) stack one Hf atom migrated to the InGaAs trough region and one row In atom migrated to the trough region. Conversely, in the a-HfO_2/InGaAs (cut II) stack, the oxide is bonded to the substrate in the trough region exclusively through oxygen atoms, producing very limited InGaAs deformation. For the a-HfO_2/InGaAs (cut I) stack the average deviation values per layer were 0.09 Å, 0.26 Å, 1.05 Å, and 1.34 Å for layers 4−7. For the a-HfO_2/InGaAs (cut II) system, the corresponding values were 0.08 Å, 0.18 Å, 0.42 Å, and 0.76 Å (Fig. 4).

The a-ZrO_2/InGaAs stacks demonstrated relatively high substrate deformation due to significant oxide-semiconductor intermixing in the row region for both cuts and partial intermixing in the trough region for cut I (Fig. 3). The average deviation values per layer were 0.14 Å, 0.29 Å, 0.90 Å, and 0.88 Å for cut I, and 0.10 Å, 0.22 Å, 0.70 Å, and 2.21 Å for cut II for the layers 4−7.

To estimate the approximate cumulative substrate deformation, the deformation curves for different stacks (Fig. 4) were numerically integrated over layers 3−7 (obtaining area below deformation curves). From the six investigated stacks, the a-Al_2O_3/InGaAs (cut I and cut II) and a-HfO_2/InGaAs (cut II) systems demonstrated the smallest cumulative InGaAs substrate deformation with integrated deformation values of 1.20, 1.03, and 1.06 Å. Conversely, the a-HfO_2/InGaAs (cut I) and a-ZrO_2/InGaAs (cut I and cut II) stacks resulted in the largest InGaAs substrate deformation with integrated deformation values of 2.07, 1.77, and 2.14 Å.

C. Bader charge analysis

Interfacial bonding can lead to a strong interface polarity and charge transfer having a negative impact on device performance. To quantify this effect, a Bader charge analysis with core correction was performed.[51,52]

1. a-Al_2O_3/InGaAs

For the a-Al_2O_3/InGaAs interfaces (Fig. 1), the Bader charge analysis shows weakly polar bond formation and no signs of ionic bonding. To compare with the XPS data, the Bader charges of the interfacial atoms were calculated relative to bulk semiconductor and oxide atoms.

Relative to bulk atoms, row As atoms bonded to Al atoms gained 0.27-0.38 |e|, row In atoms bonded to oxygen were depleted by 0.36-0.45 |e|, and row Ga atoms bonded to oxygen were depleted by 0.29 |e|. Trough Ga atoms bonded to oxygen were depleted by 0.19-0.47 |e|, while trough Ga atoms bonded to Al in cut I interface gained 0.46 |e|. Trough In atoms bonded to oxygen atoms were depleted by 0.10-0.55 |e|. Therefore, interfacial semiconductor atoms in an unpinned interface should have nearly bulk-like charges.

The analysis of the interface oxide atoms indicated that Al bonded to As had mild Bader charge gain of 0.04-0.17 |e|, and O bonded to In or Ga was depleted by 0.08-0.19 |e| vs. O and Al atoms in a-Al_2O_3 bulk. The interfacial O, an electron acceptor, was depleted of electrons relative to bulk oxide since in addition to O−Al bonds, it formed new O−In/Ga bonds; therefore, oxygen added a more electronegative (less electropositive) atom to bonding. Conversely, Al, an electron donor, gained electrons since the Al−O bonds were switched to Al−As bonds; therefore, Al atoms switched to bonding to a less electronegative atoms.

The total charge transfer from the InGaAs substrate to a-Al_2O_3 bulk through the semiconductor/oxide interfaces was calculated from the total Bader atomic charges summed up over all InGaAs atoms and bottom passivating H's in the a-Al_2O_3/InGaAs systems and comparing them with the same total charges summed up over the clean vacuum/semiconductor InGaAs(4×2)-(100) slab with bottom-passivating H atoms. The analysis of the total charge transfer through a-Al_2O_3/InGaAs interfaces showed that after formation of the a-Al_2O_3/InGaAs stacks the InGaAs slab was depleted by 1.23 |e| (cut I) and by 2.19 |e| (cut II) with limited -0.86×10^{-2} |e|/Å^2 and -1.53×10^{-2} |e|/Å^2 normalized charge transfer density. The difference in the a-Al_2O_3/InGaAs total charge transfer between cut I and cut II interfaces can be roughly explained by the number of interfacial bonds and electronegativity differences. The cut I and cut II interfaces have the same number of In/Ga−O bonds, which pull negative charge from InGaAs to the oxide; however, in comparison with cut II interface, cut I system has twice more As−Al bonds, which conversely pull negative charge back from a-Al_2O_3 to InGaAs substrate, thereby decreasing total charge transfer through cut I interface.

2. a-HfO_2/InGaAs

For a-HfO_2/InGaAs, the row As atoms bonded to Hf in the cut I and cut II systems gained ∼0.04 |e|, while those forming two weak bonds to oxygen in cut II system were depleted by 0.71-0.84 |e|, which is consistent with a high

density of As−O bonds potentially inducing poor device performance. The row As atoms forming no bonds to a-HfO_2 demonstrated charge variation from +0.14 to −0.14 |e| vs. InGaAs bulk values. The row In atoms bonded to oxygen were depleted by 0.45-0.50 |e|, while row Ga atoms bonded to oxygen were depleted by 0.22-0.45 |e|. The trough Ga atoms having bonds to oxygen were depleted by only 0.00-0.16 |e|, while trough In atoms bonded to oxygen were depleted by only 0.10-0.14 |e|.

Comparing interface oxide atom Bader charges versus bulk oxide values, interfacial Hf atoms bonded to single As gained 0.11-0.18 |e|, the Hf atom which migrated to the trough (cut I) and bonded to three As and one O gained 0.70 |e|, O bonded to In were depleted by 0.00-0.06 |e|, and O bonded to Ga were depleted by 0.00-0.10 |e|. The interfacial Hf atoms bonded to As gained Bader charge, since they switched their bonding from the more electronegative O atoms in the oxide bulk to the less electronegative As atoms in the interface. The interfacial O atoms were Bader charge depleted vs. oxide in the bulk, since in addition to O−Hf bonds, the O atoms formed new bond/s to the more electronegative In and Ga atoms.

The analysis of the total charge transfer through interface indicated that after formation of a-HfO_2/InGaAs stack, the InGaAs slab was depleted by 1.79 |e| (cut I) and 3.46 |e| (cut II) leading to -1.25×10^{-2} |e|/Å^2 (cut I) and -2.41×10^{-2} |e|/Å^2 (cut II) normalized charge transfer density through interface. The difference in the a-HfO_2/InGaAs total charge transfer between cut I and cut II interfaces can be roughly explained by a number of interfacial bonds and electronegativity difference. The cut I and cut II interfaces have roughly the same number of In/Ga−O bonds, which pull negative charge from InGaAs to the oxide; however, in comparison with cut II interface, cut I system has four times more As−Hf bonds, which pull negative charge back from a-HfO_2 to InGaAs substrate decreasing total charge transfer through cut I interface. The cut I interface has more Hf−As bonds mainly because one Hf atom migrated to the InGaAs trough region (Fig. 2).

3. a-ZrO_2/InGaAs

For a-ZrO_2/InGaAs (cut I and II) interfaces, row As atoms bonded to oxygen were depleted by ∼0.7 |e|. A single row As atom bonded to Zr gained 0.17 |e|, and row As atom completely displaced from InGaAs slab in cut I system and bonded to three oxygen atoms was depleted by 2.23 |e| value, the largest charge transfer calculated for any atom in the six oxide/semiconductor model systems. The row In atoms bonded to oxygen were depleted by 0.35-0.57 |e|, while row Ga atoms bonded to oxygen were depleted by 0.24-0.26 |e|. The trough Ga atoms bonded to oxygen were depleted by 0.07-0.34 |e|, while the trough In atoms bonded to oxygen were depleted by 0.01-0.36 |e|.

Comparing interface oxide atom Bader charges versus bulk values, interfacial Zr gained ∼ 0.05 to 0.19 |e|, interfacial oxygens bonded to In were depleted by 0.00-0.13 |e| and oxygens bonded to Ga were depleted by 0.00-0.15 |e|. The interfacial O, an electron acceptor, was depleted of electrons relative to bulk oxide, since in addition to O−Zr bonds it formed new O−In/Ga bond/s, so that oxygen added bonding to a more electronegative (less electropositive) atom. Conversely, Zr, an electron donor, gained electrons, since the Zr−O bonds were switched to Zr−As bonds, so Zr switched to bonding to a less electronegative atom.

The analysis of the total charge transfer from the substrate to the oxide indicated that for the cut I system, the InGaAs substrate was depleted by 5.49 |e| resulting in -3.82×10^{-2} |e|/Å^2 normalized charge transfer density, while for the cut II system, the substrate was depleted by 2.50 |e| or -1.74×10^{-2} |e|/Å^2 normalized charge transfer density. The difference in the a-ZrO_2/InGaAs total charge transfer between cut I and cut II interfaces can be roughly explained by a number of interfacial bonds and electronegativity difference. The cut I and cut II interfaces have the same number of Zr−As bonds, which pull negative charge from oxide to the InGaAs; however, in comparison with cut II interface, cut I system has more O−In/Ga/As bonds (13 vs. 9), which pull negative charge from InGaAs to a-ZrO_2 bulk, thus increasing total charge transfer through cut I interface.

A small charge transfer does not insure a good electronic structure. It would be expected that there should be a strong correlation between Bader charges and interface pinning/unpinning especially if there were Bader charges which greatly deviated from the bulk-like states. However, the calculations show that for the systems being studied the correlation between Bader charges and electronic structure is weak which is likely because As atoms with filled dangling bonds have near bulk-like Bader charges. Instead, the most important criteria for a good interfacial electronic structure are very limited deformation, intermixing, and substrate bond disruption which are discussed in detail below.

The comparative analysis of the investigated high-κ oxide/InGaAs interfaces demonstrates variation of total charge transfer through interface for different oxide cuts. This variation comes from slightly different number of oxide/InGaAs bonds formed in cut I and cut II interfaces, which can be explained by microscopic sizes of DFT models due to high computational cost of DFT-MD simulations. In real semiconductor devices, this variation will be eliminated by much larger statistical ensemble and the charge transfer may be dominated by processing induced defects if a disruptive oxide deposition technique is employed.

D. Coordination analysis

The interfacial coordination distribution has significant influence on interface electronic properties. The coordination perturbations can lead to creation of partially filled dangling bonds creating band-edge states, pinning the Fermi level, and deteriorating device performance. The changes in InGaAs and high-κ oxide surface coordination were investigated and compared for both cuts (cut I and cut II) of the a-Al_2O_3/InGaAs, a-HfO_2/InGaAs, and a-ZrO_2/InGaAs interfaces. Note, in computer modeling the "coordination" magnitude is determined by the number of nearest neighbor atoms within a certain cutoff radius; this can lead to a small differences in coordination number distributions in comparison with a direct imaging of electron density.

TABLE I. Coordination distribution for InGaAs surface row and trough atoms in the oxide/InGaAs stacks versus the clean InGaAs surface. Numbers in brackets correspond to atoms displaced from row or trough. Note every interface contains non-fourfold coordinated As, In, Ga atoms, but cut II a-HfO_2/InGaAs contains the highest fraction of fourfold coordinated surface atoms.

			a-Al_2O_3/InGaAs		a-HfO_2/InGaAs		a-ZrO_2/InGaAs	
		Clean InGaAs	Cut I	Cut II	Cut I	Cut II	Cut I	Cut II
Row	As	3,3,3,3	3,3,3,4	3,3,4,4	3,3,4,4	3,4,4,4	3,3,(3),4	3,3,3,4
	In	2	4	6	(5)	4	(5)	4
	Ga	2	2	3	4	3	3	(5)
Trough	As	4,4,4,4,4,4	3,3,3,4,4,4	4,4,4,4,4,4	4,4,4,4,4,5	4,4,4,4,4,4	3,3,4,4,4,4	3,4,4,4,4,4
	In	3,3	4,4	4,4	3,3	4,4	4,4	4,4
	Ga	3,3	2,3	3,4	4,4	4,4	3,(4)	4,4

The $In_{0.5}Ga_{0.5}As(100)$-(4×2) vacuum/semiconductor interface has a row/trough surface structure. The coordination distributions for InGaAs surface atoms in the DFT-MD simulated oxide/InGaAs stacks vs. the clean InGaAs surface are summarized in Table I. The InGaAs(100)-(4×2) clean surfaces have 4 As, 1 Ga, and 1 In atoms in the rows, 6 As, 2 Ga, and 2 In atoms in the troughs. The numbers in brackets in Table I indicate coordination of atoms, which were displaced from their original row or trough positions.

After stacking to a-Al_2O_3, all InGaAs atoms in the rows increased or conserved their coordination. Originally threefold coordinated As atoms increased their coordination to fourfold coordination for 25% and 50% of As row atoms for cut I and cut II, respectively. In and Ga atoms in the row increased their coordination from twofold to two-, three-, four-, and even sixfold coordination. After stacking to a-Al_2O_3, InGaAs trough atoms in some cases demonstrate coordination increase, while in other cases coordination decrease. In the cut I, a-Al_2O_3/InGaA stack, half of the As trough atoms decrease their coordination from 4 to 3, while all of the As atoms in the trough of the cut II a-Al_2O_3/InGaAs stack keep the same fourfold coordination. The In atoms in the trough increase their coordination from 3 to 4 for both cut I and cut II interfaces of a-Al_2O_3/InGaAs stack. The Ga atoms in the trough demonstrate different behavior decreasing their coordination from 3,3 to 2,3 for the a-Al_2O_3/InGaAs (cut I) stack and increasing their coordination from 3,3 to 3,4 in the a-Al_2O_3/InGaAs (cut II) interface. No significant InGaAs surface atom displacement was observed for a-Al_2O_3/InGaAs interfaces for both the cuts.

In general, in the absence of intermixing, the charge transfers were all less than one electron per semiconductor atom. This very small charge transfer for non-intermixed atoms may contrast with models of crystalline oxide/semiconductor interfaces due to the use of amorphous oxides and DFT-MD annealing/relaxation.[11,12] If a high fixed charge state is formed, and it is thermodynamically unfavorable, the high temperature annealing of the amorphous structure allows easy relaxation to a new bonding geometry with a lower total energy which usually will have a lower fixed charge. In addition, the amorphous oxide/InGaAs interfaces do not force the oxygen atoms to trade bonds from the oxide metal atoms to semiconductor atoms but instead allow for increased coordination number as explained below.

Among the three high-κ oxides, a-HfO_2 is the only oxide which does not decrease InGaAs surface atom coordination after stacking, even though it creates significant row In atom displacement for cut I system (Table I and Fig. 2). Instead, 50% and 75% of As row atoms in the a-HfO_2/InGaAs interfaces increase their coordination from threefold to fourfold for cut I and cut II, respectively, while the rest retain their original threefold coordination. The In and Ga atoms in the row increase their coordination from twofold to three-, four-, and fivefold coordination. The majority of As atoms in the trough keeps their original fourfold coordination after stacking to a-HfO_2 except one fivefold coordinated As atom. All Ga atoms in the trough after stacking to a-HfO_2 increase their coordination from three- to fourfold coordination for both cuts. For the cut I interface, all In trough atoms keep their original threefold coordination, while for the cut II interface, all In atoms increase their coordination to fourfold. The more ideal coordination distribution of a-HfO_2/InGaAs cut II vs. cut I is consistent with the better electronic structure for cut II system.

The stacking of a-ZrO_2 to InGaAs substrate created more significant perturbation and deformation in InGaAs surface than a-Al_2O_3. After a-ZrO_2 stacking, three atoms were significantly displaced from InGaAs surface in the cut I a-ZrO_2/InGaAs interface and one atom was displaced in the cut II a-ZrO_2/InGaAs interface. Average layer-by-layer deformation presented in Fig. 4 leads to similar conclusion. After stacking to a-ZrO_2, 25% of As atoms in the row increase their coordination from 3 to 4, while the remaining 75% kept the original threefold coordination. Conversely, ~33% and ~17% of As atoms in the trough decrease their coordination from four- to threefold for cut I and cut II, respectively, while the rest kept their original fourfold coordination. The In and Ga atoms in the row increased their coordination from twofold to three-, four-, and fivefold coordination forming new bonds to a-ZrO_2. The In and Ga atoms in the trough also increase their coordination from three- to fourfold coordination except one Ga atom retained its original threefold coordination.

While the previous section described the effect of oxide bonding on the coordination of substrate atoms, the next section presents the effect of substrate bonding on the coordination of interfacial oxide atoms, which is compared to the vacuum/oxide coordination.

Previously reported DFT-MD simulations of a-Al_2O_3 vacuum/oxide interfaces had surface oxygen enrichment with a roughly equal partition of two- and three-coordinated surface oxygen atoms, while the Al atoms closest to the surface had ~15% of threefold, ~75% of fourfold, and ~10% of fivefold coordination.[14]

The formation of a-Al_2O_3/InGaAs stacks (Fig. 1) changed interface coordination of the oxide atoms, thereby significantly increasing partition of threefold coordinated O atoms, and thereby increasing coordination relative to the vacuum/oxide interface. For the cut I interface, 87% of O atoms are threefold coordinated and the remaining 13% are twofold coordinated. The cut II interface has similar partitioning: 84% of O atoms are threefold and the remaining 16% are twofold coordinated. Stacking of InGaAs to a-Al_2O_3 preserved dominance of fourfold coordinated Al (92% for cut I and 55% for cut II), keeping some fivefold coordinated Al (8% for cut I and 36% for cut II), with some remnants of threefold coordinated Al (9% for cut II and 0% for cut I). This is consistent with the oxide/semiconductor interface forming by switching an Al−O bond for an Al−As bond and O atoms forming an additional O−In or O−Ga bond while retaining all original O−Al bonds.

The DFT-MD simulations of the a-HfO_2 vacuum/oxide interfaces revealed pronounced oxygen interface enrichment with twofold (~80%) and threefold (~20%) coordinated O atoms and with subsurface Hf atoms (bonded to surface O atoms) having four-, five-, six-, and sevenfold coordination (~60%, ~12%, ~24%, and ~4%).[53] The a-HfO_2 vacuum/oxide interface oxygen enrichment is very similar to the a-Al_2O_3 and a-ZrO_2 vacuum/oxide interface enrichments reported previously.[14]

The stacking of a-HfO_2 to InGaAs introduced changes in the a-HfO_2 surface coordination distributions. After stacking, O atoms shifted their peak coordination from twofold to threefold. For the cut I interface, O atoms had two- and threefold coordination (43% and 57%), respectively. In the cut II interface O atoms had two-, three-, and fourfold coordination with 12%, 82%, and 6% partition, respectively. After stacking to InGaAs, the Hf coordination peak shifted from four- to fivefold coordination. For the cut I interface, Hf atoms had four-, five-, and sixfold coordination with 10%, 60%, and 30% partition, respectively. In the cut II interface, Hf had only five- and sixfold coordination with 55% and 45% partition, respectively.

The previously published DFT-MD simulation of the vacuum/a-ZrO_2 oxide interface reported significant oxygen enrichment with the following interfacial oxide coordination: roughly equal partition or two- and three-coordinated O atoms, and subsurface Zr atoms (bonded to the surface oxygen atoms) exhibiting ~37% of fivefold and 63% of sixfold coordination.[14]

The a-ZrO_2 stacking to InGaAs changed the a-ZrO_2 coordination distribution in the interface region. For the cut I interface, the interfacial O atoms demonstrated two-, three-, and fourfold coordination (38%, 56%, 6%), respectively, while for the cut II interface, only two- and threefold coordinated O atoms (20%, 80%) were present. After stacking to InGaAs, Zr atom interfacial coordination also underwent some changes. For the cut I system, interfacial Zr atoms had four-, five-, and sixfold coordination (14%, 57%, and 29%), respectively, while interface in cut II system had only five- and sixfold coordinated Zr (55% and 45%), respectively.

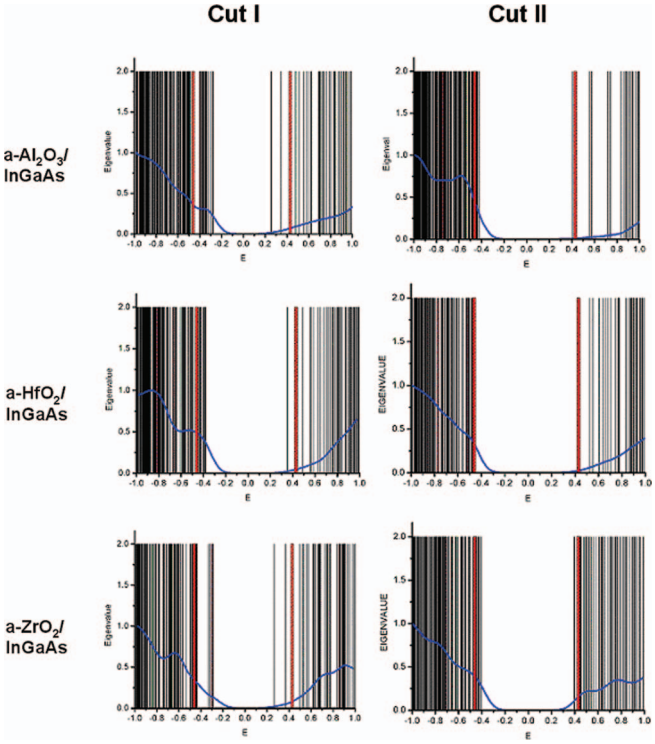

FIG. 5. Density of states and eigenvalue spectra for investigated interfaces. Red bars correspond to the bandgap of the cleaned relaxed InGaAs(4×2)-(100) slab with row-trough structure. Fermi-level corresponds to 0.0 eV.

DFT-MD simulations due to their high computational cost preclude employing large ensembles under consideration; therefore, the presented coordination partitions should be considered as rough estimates only. However, the general trends that the oxide/semiconductor interfaces formed by O atoms adding an additional O−In or O−Ga bond while retaining all original O−M (M = Al, Hf, Zr) bonds is in direct contrast to models of crystalline oxides on semiconductors where the methodology always insures that the O atoms at the interface lose bonds to oxide metal atoms while gaining bonds to semiconductor atoms.[9–12,54–57]

E. Electronic structure analysis

To investigate electronic structure of the interfaces, eigenstate spectra and density of states (DOS) curves were calculated and presented in Fig. 5. To smooth DOS curves, Gaussian smearing is often applied with a fixed Gaussian sigma parameter (0.1 eV in our case). Although Gaussian smearing provides smooth DOS curves, it also shifts valence and conduction band edges towards each other, thereby artificially decreasing the apparent bandgap value in DOS curves; this effect is more prominent in small bandgap materials such as InGaAs. To provide more accurate bandgap representation, full eigenstate spectra are plotted in Fig. 5 together with DOS curves. The eigenstates were plotted with amplitude 2.0 to reflect maximal eigenstate occupation for systems with no

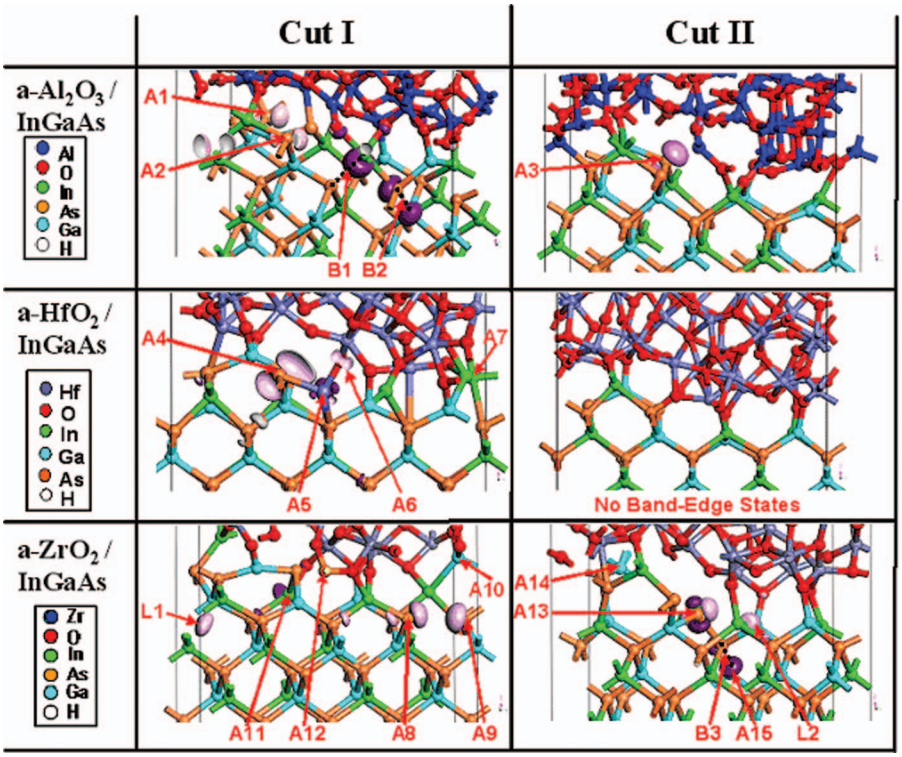

FIG. 6. Band-edge state spatial localization. Light-pink blobs correspond to valence band-edge states, while dark purple blobs correspond to conduction band-edge states.

spin-polarization. To correlate the amplitude of DOS curves plotted together with eigenstate spectra, DOS curve amplitudes were normalized to 0.0−1.0 within the −1.0 to 1.0 eV energy range (Fig. 5). The calculated bandgap values are affected by standard DFT bandgap underestimation which artificially contracts the bandgap and quantum confinement which expands the bandgap. For the present systems, these two effects partially compensate each other. A more accurate approach requires application of much more computationally expensive hybrid functionals with exact exchange, which is out of scope of this paper. The red bars in Fig. 5 represent DFT calculated bandgap (0.89 eV) of the clean relaxed InGaAs(4×2)-(100) slab with the row-trough surface structure; the red bars are included to delineate band-edge states created after interface formation and shrinking the stack total bandgap. For the reference, DFT PBE-calculated bandgap for the bulk InGaAs primitive cell is 0.50 eV. All investigated stacks demonstrate the absence of midgap states (Fig. 5). However, some of the stacks have valence and/or conduction band-edge states, which decrease interfacial bandgap value

In order to localize and investigate newly created interfacial band-edge states band-decomposed charge densities corresponding to valence and conduction band-edge states were visualized and presented in Fig. 6. The light-pink lobes in Fig. 6 correspond to valence band-edge states, while the dark-purple lobes correspond to conduction band-edge states.

1. a-Al_2O_3/InGaAs

The a-Al_2O_3/InGaAs cut I stack has a bandgap of 0.53 eV, which is less than the bandgap of the clean InGaAs(4×2)-(100) slab by 0.36 eV (Figs. 1 and 5). This bandgap decrease comes from both valence and conduction band-edge states created during interface formation. The conduction band-edge states are created by group III bond breaking "B1" (In-As) and "B2" (Ga-As) in the trough region (Fig. 6, dark-purple blobs). The valence band-edge states are localized on a row undercoordinated As atom "A2," which has no bonds to the oxide and on a fourfold coordinated row As atom "A1," which has a single bond to Al atom (light-pink blobs, Fig. 6).

The a-Al_2O_3/InGaAs cut II interface demonstrates a wider bandgap of 0.83 eV, which is only 0.06 eV less than the clean InGaAs(4×2)-(100) slab bandgap (Fig. 5). This interface has only valence band-edge and no conduction band-edge states. These valence band-edge states are localized on threefold coordinated row As atom "A3," which forms no bonds to the oxide (light-pink blob, Fig. 6). The DFT-MD simulations of a-Al_2O_3/InGaAs stack demonstrate that the main role of the oxide in forming a passive interface is to saturate the dangling bonds on the semiconductor atoms, while the bond angles, coordination numbers of the oxide atoms, and the interface polarities are secondary considerations.

2. a-HfO_2/InGaAs

The a-HfO_2/InGaAs cut I stack has valence and conduction band-edge states which lower the stack bandgap to 0.73 eV which is 0.16 eV narrower than the bandgap of the clean InGaAs(4×2)-(100) slab (Fig. 5). The migrated Hf atom "A5" has both valence and conduction band-edge states, and the O atom "A6" bonded to migrated Hf contributes to valence

band-edge states (Fig. 6). The As row atom "A4," which lost its bond to migrated out In atom "A7" and formed a new bond to the intermixed Hf atom "A5" contributes to valence band-edge states (Fig. 6).

The a-HfO_2/InGaAs cut II stack has no band-edge states revealing full bandgap of 0.89 eV identical to the bandgap of the clean InGaAs(4×2)-(100) slab (Figs. 5 and 6). This is somewhat surprising since the interface does not have ideal bonding. (a) Cut II has only 2 semiconductor atoms without 4-fold coordination consistent with a low density of 3-fold coordinated semiconductors atoms on InGaAs not always creating bandgap states. (b) The cut II a-HfO_2/InGaAs interface has no intermixing, but the interface contains two As−O bonds in addition to the more ideal Hf−As, O−In/Ga bonds consistent with a low density of weak As−O not always creating bandgap states. (c) The cut II interface has a relatively high interface dipole. For the cut I system, the total charge transfer through the interface is -1.25×10^{-2} |e|/Å^2, while for the cut II interface the same charge transfer has twice higher value of -2.41×10^{-2} |e|/Å^2. The difference in Bader charge substrate depletion between a-HfO_2/InGaAs cut I and II systems was clearly linked to compensating effects in interfacial bonding previously discussed in Subsection C II. The DFT-MD simulations of a-HfO_2/InGaAs stacks again demonstrate that the main role of the oxide in forming a passive interface is to saturate the dangling bonds on the semiconductor atoms while the bond angles, coordination numbers of the oxide atoms, interface dipoles, and even As−O bond formation are secondary considerations. The simulations show that a low density of imperfections (undercoordination and As−O bond formation) does not always cause Fermi level pining.

3. a-ZrO_2/InGaAs

The a-ZrO_2/InGaAs cut I stack has one of the narrowest bandgaps (0.56 eV) of the six model systems, which is narrower by 0.33 eV than the clean InGaAs(4×2)-(100) slab bandgap (Fig. 5). The valence and conduction band-edge states decreasing this bandgap are formed by InGaAs deformation and disruption induced during the bonding to a-ZrO_2. The valence band-edge states were localized at the undercoordinated As atoms "A8" and "A9" (note: the lobe "L1" is actually localized at As atom "A9"; however, reflection through periodic-boundary conditions visually shifted it to the other side of the cell (Fig. 6). The conduction band-edge states (dark-purple) are mainly localized at the undercoordinated In atom "A11," which lost its bond to As atom "A12" after it was pulled to the a-ZrO_2 oxide and lost all of its bonds to InGaAs substrate (Fig. 6).

The a-ZrO_2/InGaAs cut II stack had bandgap of 0.80 eV, which is only by 0.09 eV narrower than the clean InGaAs(4×2)-(100) slab bandgap (Fig. 5). The band-edge states in this system are created mainly by InGaAs deformation and bond disruption. The conduction band-edge state is localized at undercoordinated Ga atom "A15." The As atom "A13" accommodates both valence and conduction band-edge states, mainly because it lost its original bond to displaced Ga atom "A14" and had to form new As−As bonds (Fig. 6). The valence band-edge states are also localized at an In−Ga bond in the trough region. Although these Ga and In atoms are fully coordinated, they are located very close (1 bond away) from the deformation region in the trough and anomalous As−As bond formed which may contribute to their band-edge states. Comparison of the interfaces from cuts I and II for a-ZrO_2/InGaAs shows that there are subtle differences which determine if the states associated with undercoordinated atoms are just inside or outside the bandgap. The very small bandgap of the a-ZrO_2/InGaAs cut I system is consistent with intermixing itself not being a source of midgap states (i.e., intermixed As does not create midgap states in the oxide); instead, intermixing creates undercoordinated InGaAs atoms which form the midgap states.

IV. COMPARISON TO EXPERIMENTAL DATA

There are several key results from the DFT-MD simulations that can be compared to the experimental data. It is noted that there is a different scale for defects in DFT-MD, XPS, and electrical measurements. High defect densities (>5% of a monolayer) can be simulated by DFT-MD and high defect densities which have distinct chemical signatures can be detected via XPS; however, electrical measurements of interfacial traps (D_{it}) can be 10× to 100× lower. Therefore, comparison between DFT-MD simulations and XPS results are straightforward. Conversely, comparison between DFT-MD simulations and electrical data will always require consideration of the different scale of defect densities and consideration that capacitors and certainly transistors may have processing induced defects which are often not simulated in DFT-MD models. For comparison to experimental XPS data, it is important to choose interfaces in which the trap density is low by chemical standards (i.e., D_{it} less than 1×10^{13} cm^{-2}), since the processing induced defect states would be less than 1% and would not affect XPS studies.

Even with these assumptions, the DFT-MD results have several predictions which can be compared to XPS experiments. (1) All the oxide atoms in a-Al_2O_3, a-HfO_2, and a-ZrO_2 will have nearly bulk-like charges in the XPS spectra even at the interface since oxide-semiconductor bonding weakly perturbs the strong internal oxide bonds. (2) The interfacial In and Ga atoms will be mostly bonded to a single O atom and the charge loss ranges from 0.00 to 0.60 |e|. Therefore, the interfacial In and Ga atoms in XPS have a charge state which is either bulk-like or slightly more positive. (3) It is expected that the As atoms will be mostly bonded to the oxide Al, Hf, or Zr atoms and the bonds will be exceptionally weak with little charge transfer, a gain of 0.0-0.4 |e|; however, As−O bonds induce a charge loss of 0.8 |e|. Therefore, the As atoms at good oxide/InGaAs interface in XPS should be mostly bulk-like. (4) The principal electronic defects in the absence of intermixing are undercoordinated As, undercoordinated In/Ga and As−O bonds but not homo-dimers, although one As−As dimer was formed in cut II of a-ZrO_2/InGaAs. (5) There is no tendency for multi-atom intermixing once the interface is formed. Intermixing on InGaAs would show up as fully oxidized atoms such as Ga_2O_3 or In_2O_3 especially after postdeposition annealing.

There are also some predictions which can be made for electrical measurements: if intermixing and dangling bonds at the channel surface are avoided, the interfaces will have low trap density and the trap states will be very localized. Since the trap states will be localized, high mobility and slow sub-threshold swings should be readily observed not only in buried channel devices, but also in surface channel devices fulfilling these requirements. However, since nearly all current surface channel devices lack a high quality insulating gate oxide, they suffer from border traps in the oxide, fixed charge in the oxide, and interfacial fixed charge from processing induced defects all of which will lower the mobility in addition to the interfacial defects from oxide-semiconductor bonding and intermixing which also lower mobility.

The lowest oxide/semiconductor defect concentration interface may be the molecular-beam epitaxy (MBE) grown interface between Ga_2O_3 and GaAs(001)-2×4 which is grown via deposition of Ga_2O from a Ga_2O_3 source.[58–61] Recent *in situ* XPS and reflection high-energy electron diffraction (RHEED) studies by Priyantha *et al.*[62] as well as Hinkle *et al.*[63,64] of this Ga_2O_3/GaAs(001) interface showed that the Ga_2O forms an ordered overlayer, and this ordered overlayer was previously observed in scanning tunneling microscopy (STM) by Hale *et al.*[61] The XPS shows only bulk-like As and no As−O bonds. The only non-bulk Ga peak is shifted by 0.5 eV to higher binding energy and assigned as Ga^{+1} from Ga_2O consistent with the formation of Ga−O surface bonds and no O back-bonds which was also observed in STM and DFT models.[61,65] These results are consistent with the DFT-MD results observed in this paper for amorphous oxide-InGaAs bonding modeling. (1) Formation of In/Ga−O bonds does not create bandgap states; (2) an unpinned interface needs to have a minimum of dangling bonds; (3) an unpinned interface does not contain high concentrations of Ga^{+3} or As dimers. Comparisons to ALD interfaces are a bit more complicated since there is a wide variety of processing conditions and the bulk oxides often contain fixed charge and border traps.

A. a-Al_2O_3/InGaAs

Milojevic *et al.* used *in situ* monochromatic XPS with a 45° takeoff angle to study the interfacial bonding after 1/2 cycles of trimethyl aluminum (TMA) and H_2O were dosed on InGaAs(100) substrates between 200 °C and 300 °C which had been cleaned with $(NH_4)_2S$ (Ref. 66). For XPS shifts, the bulk oxide and semiconductor bulk states were used as reference states; the bulk InGaAs were assigned as In^{+0}, Ga^{+0}, and As^{+0}, while Al_2O_3 were assigned as Al^{+3} and O^{-2}. The samples already had surface oxygen prior to the 1st TMA pulse in the form of Ga−O, In−O, and As−O so the Al was Al^{+3} even after the first pulse. Two TMA pulses almost eliminated Ga^{+3}, but the Ga^{+1} peak was only reduced to ∼0.15 M for all temperatures studied. For 300 °C ALD, TMA removes the As−S bonds. At both 200 °C and 300 °C, TMA removes all As−O bonds, but the TMA As−O bond removal occurs more rapidly at 300 °C. There is a high residual coverage of As−As which may be due to the reduction of As oxides by TMA; note there are substantial As oxides and maybe even As_2 on the initial surfaces due to air exposure and lack of pre-annealing. The data are consistent with the DFT-MD results in this paper showing: (1) there is no tendency to form As oxides upon Al_2O_3/InGaAs annealing, (2) the interfacial As atoms have no significant net charge, (3) charge transfer from Ga to the oxide is limited to one electron per atom, and (4) there is no tendency for substantial intermixing.

A similar experiment was performed by Aguirre-Tostado *et al.*[67] on samples using atomic hydrogen at 450 °C surface temperature to remove native oxides instead of NH_4S wet cleaning.[68] A Ga^{+1} XPS peak found at the interface was assigned to Ga−O bonding since no sulfur was present. The Ga−O bonds at the interface can be assigned either to residual substrate oxides or bonding between a-Al_2O_3 and the substrate. This surface cannot be directly compared to DFT-MD simulations in the present paper since cleaning by atomic hydrogen can deplete the surface of In. However, these experiments correlate well with DFT-MD predictions that the bonding between a-Al_2O_3 and InGaAs is sufficiently weak, that the As, Al, and O charge states are bulk-like, and that the Ga is slightly shifted due to the loss of a partial charge.

In a similar study, Kirk *et al.*[69] used *in situ* XPS to study the interfacial bonding after 1/2 cycles of TMA and H_2O were dosed on InAs(100) substrates at 300 °C which had been cleaned either in $(NH_4)_2S$ or NH_4OH. This study is particularly important in understanding if In surface atoms will have different properties than Ga surface atoms. In general, $(NH_4)_2S$ is more efficient than NH_4OH in preventing InAs oxidation prior to ALD during sample transfer and pump down in the ALD system, but heating at 300 °C shifts the S XPS peak and removes all As−S bonds which Kirk *et al.* attribute to some subsurface adsorption complicating the data interpretation. TMA exposure of the $(NH_4)_2S$-treated surface does not change the O XPS intensity, but TMA exposure of the NH_4OH-treated surface does reduce O XPS intensity on NH_4OH-treated samples. The TMA reduced the In^{+3} very efficiently, but the In^{+1} peak persisted; however, there was very little In^{+3} on the wet cleaned surfaces compared to Ga^{+3} on wet cleaned GaAs. The $(NH_4)_2S$-cleaned surface after TMA had only bulk-like As charge states consistent with the DFT-MD results in this paper. The NH_4OH surface had formed significant surface oxide prior to ALD and after ALD had a much greater As−As concentration consistent with the As−As being mostly a product of reduction of surface oxides by TMA or being present in the air-exposed surface and not primarily a product of oxide-InAs bonding which is consistent with the DFT-MD results presented in this paper; note, however, one As−As formed in cut II of a-ZrO_2/InGaAs in the present study. Kirk *et al.*[69] observed no XPS binding energy shift for As−Al bonds again consistent with the DFT-MD results presented in this manuscript.

Trinh *et al.*[70] using C-V and XPS have studied the interface of ALD Al_2O_3/InGaAs using different surface treatment and post-deposition annealing (PDA) techniques. They wet cleaned the surface with $(NH_4)_2S$ and subsequently employed 10 half-cycles of TMA at 300 °C to condition the surface prior to TMA + H_2O Al_2O_3 growth at 300 °C. PDA in N_2 vs. H_2 was compared at 500 °C prior to gate metal deposition. After gate metal deposition, a second PDA in N_2 at 400 °C was performed. The C-V showed that the sulfur pre-treatment lowers

the D_{it}. With H_2 PDA, the typical inversion bump in CV is consistent with an especially low D_{it}. The XPS shows that without $(NH_4)_2S$ cleaning and TMA pre-treatment, cleanup is incomplete and there are interfacial oxide. However, with $(NH_4)_2S$ cleaning and TMA pre-treatment, cleanup is nearly complete. The XPS also shows the main role of H_2 PDA is removal of As_2O_3. However, even for the $(NH_4)2S$-cleaned, TMA-pretreated, and H_2 PDA samples there is Ga_2O_3 and In_2O_3 at the interface but no AsO_x. Again this is consistent with the interfacial oxides being due to imperfect ALD cleaning and not due to oxide/InGaAs reactions.

Shin *et al.*[71] as well as Kim *et al.*[72] have studied the interfacial bonds between Al_2O_3/InGaAs using *in situ* XPS experiments for ALD of Al_2O_3 using TMA and H_2O on decapped InGaAs, thereby avoiding the issues of remnant oxides from the air exposed wafers and As_2 (arsenic dimer) formation from TMA reduction of arsenic oxides. The ALD system employed by Shin *et al.* has a high vacuum base pressure, unlike some commercial ALD tools, thereby further reducing any background oxidant exposure. They did not observe any gallium or arsenic oxides at the Al_2O_3/InGaAs interface consistent with the DFT-MD simulations showing nearly all semiconductor atoms have bulk-like charge. It should be noted that they did not have monochromatic XPS, and Shin *et al.* did not detect appreciable Ga^{+1} or As_2 when Al_2O_3 was grown by ALD on carefully wet cleaned InGaAs which had been pre-annealed to remove any arsenic oxides prior to ALD.[73] While As_2 is relatively easy to detect with standard XPS, the chemical shift for Ga^{+1} is quite small; therefore, it is possible that they may not be sensitive for detection of very small amounts of Ga^{+1}. However, Kim *et al.*[72] also employed HRTEM, high-angle angular dark-field (HAADF) TEM to demonstrate that a chemically abrupt interface of a-Al_2O_3/$In_{0.53}Ga_{0.47}As$(100) is formed by *in situ* decapping of As_2-capped $In_{0.53}Ga_{0.47}As$(100) followed by a-Al_2O_3 ALD.[74,75]

The present study employed an In/Ga rich reconstruction which greatly reduces the likelihood of As−As dimer formation. The crystalline models usually employ a bulk termination which might facilitate As−As defect formation. However, we note that the experimental C-V work of Hwang *et al.* (see Ref. 50) shows that for high temperature trimethyl aluminum first oxide growth, the As-rich 2×4 reconstruction provides a better interface consistent with the propensity of TMA to bond at As−As sites as noted in the STM work of Clemens *et al.* (see Ref. 76) and Melitz *et al.* (see Ref. 77). Melitz *et al.* show that the 4×2 surface is passivated by TMA up to 200 °C, while the 2×4 surface is passivated by TMA up to 300 °C because of elimination of As−As dimer bonds by TMA.[77] It is noted that the oxide growth experiments by Hwang *et al.* were performed on pristine surfaces and not on typical air-exposed surfaces.[50] Therefore, the experimental work on pristine clean surface is also consistent with the As−As not being formed by bonding to gate oxide.

There is also an *in situ* XPS study for ALD of Al_2O_3 on *in situ* grown GaAs(100)-(4×6) by Chang *et al.*[78] In contrast to the work of Shin *et al.*,[71] Chang *et al.* used a commercial ALD reactor; therefore, the samples were exposed to some background oxidants. The XPS spectrum only showed small amount Ga^{+1} and As−As, but neither showed Ga^{+3} nor showed arsenic oxides. Hinkle *et al.* used monochromatic XPS studies *in situ* on a decapped GaAs-(2×4) samples.[63] Using MBE of Ga_2O on the decapped samples, they saw only Ga^{+1} at the interface, no interfacial arsenic oxides, no As_2, and no Ga^{+3}. This is in contrast to NH_4OH-treated surfaces which have Ga^{+3} from Ga_2O_3 as well as Ga^{+1} from Ga_2O. Hinkle *et al.* did not ALD deposit Al_2O_3 onto decapped GaAs nor decapped InGaAs; instead, they used wet cleaned surfaces for ALD deposition. However, on their best cleaned surfaces, they observed that the electrically optimized oxide/GaAs interfaces always only had Ga^{+1} and no Ga^{+3}, no As_2, and no arsenic oxides. This is consistent with the DFT-MD results in this manuscript showing that the Ga in the interface is bonded to only one oxygen and produces a minimal charge change.

Kim *et al.*[72] performed C-V measurements of a-Al_2O_3/$In_{0.53}Ga_{0.47}As$(100) stacks formed by *in situ* decapping, with a forming gas PDA indicating strong inversion at elevated temperatures, consistent with an unpinned a-Al_2O_3/InGaAs(100) interface.[74,75] DFT modeling by Weber *et al.*[79] indicates that the hydrogen passivation primarily eliminates defects in the oxide as opposed to the interface. The electrical experimental data by Kim *et al.* correlate well with the presented DFT-MD simulations demonstrating abrupt interface with no intermixing, nearly weak covalent bonding between a-Al_2O_3 and InGaAs(100) with chemical shifts of less than one electron for all interfacial atoms. Nearly all other studies of oxide/InGaAs interfaces employed only wet cleaned samples; therefore, one cannot expect XPS to show a low residual oxide content at the interface.

Huang *et al.*[80] have shown that the processing induced defects of ZrO_2/$In_{0.53}Ga_{0.47}As$ MOSFETs can be controlled by using an amorphous (La)AlO_x interlayer between the ZrO_2 and the semiconductor substrate. The interlayer reduced border traps, interface traps, and oxide fixed charge. The interfacial structure between (La)AlO_x and InGaAs is likely to be very similar to that between Al_2O_3 and InGaAs, which is consistent with DFT calculations showing the interface is passive in the absence of any processing induced intermixing. Scanning tunneling microscopy and spectroscopy studies (STS) by Clemens *et al.*[76] show that a-Al_2O_3/InGaAs interfaces are likely to have the fewest processing induced defects because TMA dissociatively chemisorbs to form an ordered monolayer without displacing any surface substrate atoms; there are no known analogous ALD precursors for HfO_2 and ZrO_2.

Transistor device results from Xuan *et al.* for surface channel a-Al_2O_3/InGaAs prepared by wet cleaning of the substrate show very high output current, low threshold voltage, reasonable sub-threshold swing, and reasonably low off current for submicron devices.[81–83] Recent transistors results by Egard *et al.*[84] for a surface channel L_g = 150 nm a-Al_2O_3/$In_{0.53}Ga_{0.47}As$ prepared by wet cleaning of the substrate show sub-threshold (SS) swings of only 77 mV/dec at V_{DS} = 50 mV and 100 mV/dec at V_{DS} = 0.5 V consistent with low D_{it}. In general, the device results for high In content, low bandgap channels are better than for GaAs with high bandgap channels due to either chemical bonding effects (i.e., better oxide passivation of

semiconductor dangling bonds) or band offset effects (oxide defects are outside the semiconductor bandgap), or favorable defect energy levels (semiconductor defects states are outside the semiconductor bandgap).[85,86] For $In_{0.65}Ga_{0.35}As$ 400-nm gate-length enhancement-mode devices, G_m (extrinsic, $V_{DS} = 2V$) = 350 mS/mm, $V_T = 0.4$ V, SS = 350 mV/dec, and $I_{on}(V_{GS} = 4\ V)/I_{off}(V_{GS} = 0\ V) = 150$.[83] Although the sub-threshold swing was large and I_{on}/I_{off} was modest, the output currents were high and scaled with gate length. Xuan *et al.*[82] obtained better results with higher indium content devices.[87] For $In_{0.75}Ga_{0.25}As$ 750-nm gate-length enhancement-mode devices, G_m(extrinsic, $V_{DS} = 2V$) = 430 mS/mm, $V_T = 0.5$ V, SS = 190 mV/dec, and $I_{on}(V_{GS} = 1\ V)/I_{off}(V_{GS} = 0\ V) = 10^6$. The large sub-threshold swing is ascribed to problems associated with the implanted source/drain contacts in addition to interface traps (note there are several studies on regrown source drains showing a pathway for low access resistance).[88] For gate lengths less than 200 nm, lower sub-threshold swings are observed (100 mV/dec). The results by Xuan *et al.* are consistent with DFT showing that there can be a low density of states at the interface with optimal processing and that most defect states only locally perturb the electronic structure. It is noted that much higher 10× interfacial states density has been observed by Caymax *et al.*[89] for a-Al_2O_3/GaAs using TMA and H_2O with a 300 °C forming gas anneal which is consistent with TMA, creating a high interfacial state density when the substrate is disrupted during processing.

Extremely high mobilities have been obtained for buried channel a-Al_2O_3/$In_{0.7}Ga_{0.3}As$ MOSFETs. Zhao *et al.*[90] have reported mobilities of 4400 cm^2/V sec, low sub-threshold swings of 106 mV/dec using a 4 nm InP barrier layer with ALD deposited a-Al_2O_3. However, even without the InP barrier, the sub-threshold swing was only 118 mV/dec. Very recently, Bentley *et al.*[91] observed similar mobilities of 6600 cm^2/V s in a buried channel device and a 4300 cm^2/V s in a surface channel device at a carrier density of 3×10^{12} cm^{-2} using ALD a-Al_2O_3/$In_{0.53}Ga_{0.47}As$ MOSFETs in a flatband transistor design. Radosavljevic *et al.*[92] using both buried channel and a FinFET design with a $TaSiO_x$ gate dielectric have observed sub-threshold swings as low as 73 mV/dec.[93] These results are consistent with DFT calculations showing that in the absence of intermixing and semiconductor oxidation, a low density defect states only cause a local perturbation of the electronic structure; however, it is noted that electrical measurements from MOSFET results are strongly influenced by processing induced defects in the oxide, contacts, and gate.

B. a-HfO_2/InGaAs

For HfO_2 there is little XPS data on HfO_2/InGaAs, but there are several XPS studies on the amorphous HfO_2/GaAs interface. Suri *et al.*[94] investigated the bonding at the HfO_2/GaAs(100) interface after ALD deposition of HfO_2 using TDMAH ($Hf(NMe_2)_4$) and H_2O from 200 °C to 300 °C with *ex situ* XPS. All experiments were performed on GaAs(100) with native oxide without a wet pre-clean. By increasing the ALD temperature to 300 °C, the TMA self-cleaning eliminated all XPS As oxide peaks. However, there was a non-bulk As peak attributed to As^0 which was ascribed to As_2, a reduction in Ga^{+3}, and little reduction in Ga^{+1}. Suri *et al.* attributed the As_2 formation to oxygen transfer from AsO_x to Ga_2O_3. Most importantly, post-deposition annealing did not increase interfacial oxide content but decreased interfacial arsenic oxide content that remained after low temperature (200 °C) ALD. The data are consistent with several of the DFT-MD results in this manuscript: (1) there is no tendency to form As oxides and (2) the interfacial As atoms have no significant net charge. The As−As bonding at the interface in this paper by Suri *et al.* is likely just a consequence of the tetrakis(diethylmethylamino) hafnium (TDMAH) reduction of native oxides and might not be present for oxides gently deposited on pristine samples.

Chang *et al.* using highly surface sensitive synchrotron XPS and TEM confirm that the Ga^{+3} at the HfO_2/InGaAs is from incomplete reduction of native oxides as opposed to intermixing.[95] Chang *et al.* used 7.8 nm thick ALD-HfO_2 films deposited on air-exposed $In_{0.53}Ga_{0.47}As$/InP which had a native oxide surface layer. The ALD growth was carried out at a wafer temperature of 200 °C using tetrakis-ethylmethylamino-hafnium (TEMAH) and H_2O. Prior to HfO_2 ALD, As−O, In−O, and Ga−O bonding is observed; after ALD, only trace In−O and Ga−O bonding is observed, and most of the interfacial atoms had bulk-like bonding consistent with the DFT-MD results presented in this manuscript. The trace oxide may be due to the deposition being performed on native oxide.[95,96] Similar TEMAH ALD XPS studies were performed by Suh *et al.* on native oxide covered GaAs with a PDA at 500 °C and 700 °C in N_2 and NH_3. They found only Ga−O bonding and no As−O bonding. The GaO_x content increases upon PDA annealing consistent with GaO_x diffusing into the oxide. However, interfacial layer formation can occur depending on the wet cleaning method and the ALD precursor.[97] The results by Chang *et al.* and Suh *et al.*[98] are consistent with the DFT result showing a preference for O−Ga/In bond formation over O−As bond formation.

There is one study on formation of a-HfO_2/InGaAs interfacial in UHV on a decapped sample, thereby insuring no native oxides are present. Hwang *et al.*[99] used C-V and conductance to study the interface between CVD HfO_2 grown on a seed layer formed by trimethyl aluminum on decapped InGaAs(100) in an oxygen free atmosphere. After forming gas anneal, studies on metal-oxide-semiconductor capacitor (MOSCAP) devices show that the Fermi level is unpinned, the C-V data on n-type InGaAs(100) has very low dispersion compared to most other published data, and the inversion peak from trap states is very small compared to most other published data. This is consistent with the DFT-MD results in this manuscript showing that the HfO_2/InGaAs(100) interface is thermodynamically stable and not prone to intermixing and that the source of pinning states is dangling bonds since they are likely to be passivated by hydrogen.

Oktyabrsky *et al.*[100] studied deposition of HfO_2 via e-beam deposition of Hf in an O_2 ambient. For processing below 600 °C, no interfacial control (IFC) layer is required to prevent intermixing. A buried channel device HfO_2/$In_{0.53}Ga_{0.47}As$ (2 ML)/$In_{0.52}Al_{0.48}As$/$In_{0.53}Ga_{0.47}As$/InP with an equivalent oxide thickness (EOT) of 2.9 nm was studied.

For this device, the threshold voltage was only +0.15 V, the sub-threshold swing was 150 mV/dec corresponding to a trap density of 1.3×10^{13} cm^{-2} eV^{-1}, and the mobility measured using the Hall technique was 1800 cm^2/V s at a sheet density of 3×10^{12} cm^{-1} which is close to the bulk mobility of $In_{0.53}Ga_{0.47}As$ with a doping of 10^{18} cm^{-3}. The results are quite impressive considering that the deposition process will result in some oxidation of the $In_{0.53}Ga_{0.47}As$ capping layer due to the O_2 ambient and the use of uncapped wafers. These experimental results are consistent with the DFT-MD calculation showing a-HfO_2 can form an unpinned interface on InGaAs if processing induced intermixing is avoided. The results are also consistent that pinning states are nearly confined to the first monolayer of semiconductor if process induced intermixing is avoided.[100] Scanning tunneling microscopy and spectroscopy work by Clemens *et al.* on direct e-beam deposition of HfO_2 onto InGaAs(100)-(4×2) from a HfO_2 target in UHV shows at least partially unpinning of the Fermi level; the authors speculate that residual defect states are induced by oxygen from the incongruent e-beam evaporation of HfO_2.[101] Electrical measurements, TEM, and RHEED measurements by Chang *et al.*[102] for crystalline HfO_2/InGaAs(100) deposited by e-beam of HfO_2 confirm that there is no tendency for intermixing at the c-HfO_2/GaAs(100) interface and show a low density of states near the valence band edge.

Xuan *et al.*[81] have fabricated surface channel inversion enhancement mode surface $In_{0.65}Ga_{0.35}As$ MOSFETs with a 8 nm a-HfO_2 gate oxide deposited directly on the $(NH_4)_2S$ wet cleaned InGaAs channel by ALD with a postdeposition anneal at 400–500 °C in N_2.[103] The threshold voltage was 0.6 V, the drain current was 1.0 A/mm, and the transconductance was 0.37 S/mm at a drain voltage of 2 V. After subtracting the contact resistance, the Xuan *et al.* estimated the performance was as high as 1.5 A/mm and 0.57 S/mm both of which scaled with gate length. Xuan *et al.* state that the performance is almost identical to similar devices with ALD Al_2O_3 gate oxide. The ALD $HfO_2/In_{0.65}Ga_{0.35}As$ performance is consistent with at least a partial unpinning of the Fermi level in some of the channels. Again, the high output currents are consistent with any pinning states being confined to the first monolayer of the oxide/semiconductor interface. Chang *et al.* reported D_{it} as low as 1 to 2×10^{12} cm^{-2} eV^{-1} near midgap for InGaAs MOSCAPs with ALD HfO_2 gate oxide formed using TEMAH and H_2O at 200 °C followed by a forming gas anneal even with a residual 0.5 nm of native oxide;[95] however, Caymax *et al.* performed careful variable temperature C-V studies on GaAs showing that ALD HfO_2 gate oxide formed using $HfCl_4$ and H_2O and a 300 °C forming gas anneal have a D_{it} of 3×10^{13} cm^{-2} eV^{-1} near midgap probably due to substrate disruption during ALD;[89] it is noted that halogen containing precursors should be highly disruptive to the lattice due to halogen induced etching; Caymax *et al.* results are consistent with low defect interfaces requiring very gentle oxide deposition conditions.

C. a-ZrO_2/InGaAs

Koveshnikov *et al.*[104] used XPS to study the interface of ALD ZrO_2 on InGaAs. The ALD gas is not given. The authors state the interfaces are stable to 800 °C and no interfacial layer is observed in TEM and TEM- electron energy-loss spectroscopy (EELS). PDA was performed at 350 °C. Oxide physical thicknesses were 5, 7, 10, and 15 nm. *Ex situ* depth profiling XPS shows no shift in any of the In, Ga, or As peaks consistent with no oxidation of InGaAs and the high thermodynamic stability of the interface observed in the DFT-MD studies.

Koveshnikov *et al.*[104] fabricated long channel (3−10 μm) n-MOSFET with 5 nm ALD a-ZrO_2 gates.[105] The surface channel MOSFET had a threshold voltage of +0.25 V, a sub-threshold swing of 100 mV/dec, and a channel mobility of 2270 cm^2/V s at $V_g = 0.45$ V and a sheet carrier density of 2×10^{11} cm^{-2}; the channel conduction in the linear region was as high as 490 mS/mm. The device data are consistent with DFT-MD results in this manuscript showing that any interfacial pinning states have only a local effect on the electronic structure, while the XPS data are consistent with DFT results showing that the interface is dominated by covalent bonding with minimal charge transfer.

Stemmer *et al.*[106] fabricated MOSCAP with ALD a-ZrO_2 using zirconium tetra-tert-butoxide (ZTB) and H_2O at 300 °C with a 350 °C forming gas PDA. Using HAADF/STEM TEM, the authors observe an abrupt interface with no intermixing. C-V analysis was performed to determine the quality of the oxide; minimal frequency dispersion (1.3% to 1.9% per decade of frequency) with a nearly ideal flatband voltage was observed. Even as a function of temperature, no dispersion in accumulation and depletion was observed consistent with a low D_{it}. These results are consistent with the DFT-MD simulations in this manuscript, thus showing that there is no substantial intermixing at the a-ZrO_2/InGaAs interface and any low density pinning states have a very localized effect in the absence of intermixing and semiconductor oxidation on the electronic structure in the absence of processing induced intermixing.

V. COMPARISON TO CRYSTALLINE OXIDE/GaAs MODELS

There are no published DFT studies of even crystalline oxide/InGaAs interfaces. However, there are published DFT studies of c-HfO_2/GaAs interfaces. It is noted that comparison to the present study is limited by several factors: (a) The crystalline models used a bulk termination, which is not a specific experimental reconstruction. (b) The crystalline models used DFT relaxation at 0 K instead of DFT-MD annealing at finite temperature, thereby limiting the relaxation around defects. (c) In general, the crystalline polymorphs are much less flexible than the amorphous systems, so there will be limited atomic motion during relaxation of the assumed bonding structure. (d) The crystalline models sometimes have lower coordination of oxide atoms at the semiconductor interface than in the bulk oxide. It is noted that the crystalline oxide models have been very successful in understanding defect structures even in amorphous oxides.[54,79]

Even with these differences, the DFT-MD results have several predictions which can be compared to crystalline oxide models. (1) All oxide atoms in a-Al_2O_3, a-HfO_2, and

a-ZrO_2 will have bulk-like Bader charges even at the interface since oxide-semiconductor bonding weakly perturbs the strong internal oxide bonds. (2) The interfacial In and Ga atoms will be mostly bonded to a single O atom and the Bader charge loss ranges from 0.00 to 0.60 |e|. (3) It is expected than the As atoms will be mostly bonded to Al, Hf, or Zr atoms and the bonds will be exceptionally weak with little charge transfer, a gain of 0.0-0.4 |e|; however, As−O bonds induce a charge loss of 0.8|e|. Therefore, the As atoms at good oxide/InGaAs interface should be mostly bulk-like. (4) The principal electronic defects in the absence of intermixing are undercoordinated As, undercoordinated In/Ga, and As−O bonds but not homo-dimers although one As−As dimer was formed in cut II a-ZrO_2/InGaAs(100) interface. (5) There is no tendency for multi-atom intermixing once the interface is formed.

Wang *et al.*[11] have employed VASP PW91 DFT modeling to study the effect of oxygen depletion at the crystalline HfO_2(001)/GaAs(001) interfaces and crystalline Al_2O_3/GaAs(001) interfaces formed by Ga−O bonding.[55] In these calculations, the c-HfO_2 was rotated by 28.04° so that it was nearly lattice matched to GaAs minimizing interfacial strain. The authors found that oxidation resulted in the formation of various defect states. For c-HfO_2/GaAs(001), a Ga−O interface was employed which generated defects including As−As dimer and Ga dangling bonds. Wang *et al.* found that the Ga dangling bond gave a state at the conduction band edge, consistent with the results in the present manuscript. They also simulated two defects which are not commonly found in the DFT-MD simulations of the amorphous oxide-InGaAs(100)-(4×2) interfaces (As−As dimers and Ga^{+3} states), so a comparison is not possible. It is noted that the one As−As dimer formed in cut II of the a-ZrO_2/InGaAs interface formed both conduction and band edge states which is also roughly consistent with the results of Wang *et al.* after considering the smaller bandgap of InGaAs vs. GaAs.

Wang *et al.*[12] have used VASP with PW91 to model HfO_2(001)/GaAs(001) with a double interface and no vacuum space with a lattice mismatch of 10% which reduces the calculated bandgap of HfO_2 by 1.3 eV. Four separate bulk terminated interfaces were modeled with O−Ga, O−As, Hf-Ga, and Hf−As bonds. The DFT models show that the most stable interface is formed by Ga−O bonds and the least stable interface is formed by O−As which is consistent with our DFT-MD results showing that for the amorphous oxides the most common bonds are O−Ga/In and the metal−As bonds are more prevalent than the O−As bonds. Note that in the most stable crystalline model, there are only O−Ga bonds and no oxide-As bonds which are sometimes present in the amorphous oxide-InGaAs DFT-MD simulations. An experimental study of the crystalline interface between HfO_2 and the group III-rich InGaAs(001)-4×2 was carried out by Chang *et al.*[102] The C-V measurements by Chang *et al.*[102] showed low dispersion consistent with an unpinned interface. In agreement with the model by Wang *et al.*, no intermixing or deformation was found at the c-HfO_2/InGaAs interface.

Robertson and coworkers have employed crystalline models of Al_2O_3 and HfO_2 on bulk terminated GaAs(001) to determine the source of midgap states.[10,56,57] A double interface model with no vacuum was employed along with CASTEP generalized gradient approximation (GGA) ultrasoft pseudo-potential calculations. For the bulk-terminated surface, the GaAs(100) surface is either 100% Ga or 100% As terminated; therefore, there are always dangling bonds with a non-integer number of electrons. When an interface is formed via Ga−O bonds, the Fermi level lies in the valence band. The problem can be relieved by substituting oxygen for 50% of the subsurface As sites (O_{As}) or substitute Ga for 50% of the subsurface Hf sites (Ga_{Hf}) to give an unpinned interface. It is noted by Robertson *et al.* that these substitution defects are not required for trivalent oxides such as c-Al_2O_3 for both bulk Ga and As terminated GaAs(100). These results cannot be directly compared to the DFT-MD simulations of amorphous oxides on InGaAs(100)-(4×2) since the amorphous oxide interface atoms are free to be fully coordinated to other oxide atoms, thereby forming only weak bonds to the semiconductor. However, Robertson *et al.* also simulated various defects for c-HfO_2/GaAs as well as for c-Al_2O_3/GaAs. For c-HfO_2/GaAs(100)-(1×1) and c-Al_2O_3/GaAs(100)-(1×1), they found As dangling bonds forming states just inside valence band edge, Ga dangling bonds forming states just inside or outside the conduction band edge, and As−O bonds not forming bandgap states similar to the DFT-MD results for amorphous oxide/InGaAs in this paper. In general, the authors note that if the bonds are fully relaxed then the dangling bond states are outside the bandgap. We note that Robertson *et al.* found that for c-Al_2O_3/GaAs(100)-(1×1) the Ga−Ga dimer bonds formed defect states just below the valence band edge, which is in disagreement with the results given in this paper. Robertson *et al.* also studied the energy of the defect states as a function of the bandgap by examining GaAs, InAs, and InP. Since the valence bands of the semiconductors are aligned, the Ga dangling bond state is found to be fully inside the conduction band for InAs.

VI. CONCLUSION

Comprehensive DFT-MD simulations of a-Al_2O_3/InGaAs, a-HfO_2/InGaAs, and a-ZrO_2/InGaAs interfaces were performed using realistic high-κ oxide samples to investigate interface formation, bonding structure, and electronic properties at atomistic level. The a-Al_2O_3/InGaAs stacks annealed at 800 K demonstrate good interface properties with no intermixing, low interface charge transfer, and low InGaAs deformation. The interface atoms demonstrate Bader charges very close to the in-bulk values in correlation with XPS chemical shift data. The a-HfO_2/InGaAs stacks can form unpinned interfaces; however, they have a propensity towards band-edge state creation because of Hf atoms migrating to InGaAs troughs in addition to moderate substrate deformation and medium interface polarity. The a-ZrO_2/InGaAs interfaces demonstrate enhanced interface intermixing, substrate deformation and interface polarity, and definitely require some kind of passivation treatments to make these interfaces usable in microelectronics applications. All investigated stacks demonstrate unpinned interfaces; however, some of the interfaces have band-edge states leading to bandgap

shrinkage. The band-edge states were mainly produced by InGaAs deformation, bond disruption, and intermixing, and they were predominantly localized on undercoordinated As atoms for valence band edge states and improperly bonded In and Ga atoms for conduction band edge states. The DFT-MD simulations are consistent with a weak bonding between the oxide and the semiconductor, which is very desirable for obtaining an unpinned interface between a highly ionic metal oxide and a compound semiconductor with low interface intermixing and substrate deformation. This can be achieved if the oxide deposition technique does not create significant substrate deformation/intermixing and leads to interface with very few partially filled dangling bonds, which are far more reactive than the filled or empty dangling bonds.

ACKNOWLEDGMENTS

We would like to thank Intel, MARCO, and the SRC for support, and Paul McIntyre, Robert Wallace, Christopher Hinkle, and Matthias Passlack for useful discussions.

[1]G. Nicholas, T. J. Grasby, D. Lgoni, C. S. Beer, J. Parsons, M Meuris, and M. M. Heyns, IEEE Electron Dev. Lett. **28**, 825 (2007).
[2]S. Takagi, T. Tezuka, T. Irisawa, S. Nakaharai, T. Numata, K. Usuda, N. Sugiyama, M. Shichijo, R. Nakane, and S. Sugahara, Solid-State Electron. **51**, 526 (2007).
[3]E. J. Kim, E. Chagarov, J. Cagnon, A. C. Kummel, P. M. Asbeck, S. Stemmer, K. C. Saraswat, and P. C. McIntyre, J. Appl. Phys. **106**, 124508 (2009).
[4]K.-Y. Tse and J. Robertson, J. Appl. Phys. **100**, 093713 (2006).
[5]J.-H. Ha, K.-I. Seo, P. C. McIntyre, K. C. Sarawat, and K. Cho, Appl. Phys. Lett. **90**, 112911 (2007).
[6]P. Broqvist and A. Pasquarello, Microelectron. Eng. **84**, 2022 (2007).
[7]J. Godet, P. Broqvist, and A. Pasquarello, Appl. Phys. Lett. **91**, 262901 (2007).
[8]P. Broqvist, A. Alkauskas, and A. Pasquarello, Appl. Phys. Lett. **92**, 132911 (2008).
[9]J. Robertson and L. A. Lin, Microelectron. Eng. **88**, 373 (2011).
[10]L. Lin and J. Robertson, Appl. Phys. Lett. **98**, 082903 (2011).
[11]W. C. Wang, K. Xiong, R. M. Wallace, and K. Cho, J. Phys. Chem. C **114**, 22610 (2010).
[12]W. C. Wang, K. Xiong, G. Lee, M. Huang, R. M. Wallace, and K. Cho, Appl. Surf. Sci. **256**, 6569 (2010).
[13]E. Chagarov and A. Kummel, Surf. Sci. Lett. **602**, L74 (2008).
[14]E. A. Chagarov and A. C. Kummel, J. Chem. Phys. **130**, 124717 (2009).
[15]E. A. Chagarov and A. C. Kummel, ECS Trans. **16**, 773 (2008); Surf. Sci. **603**, 3191 (2009).
[16]See supplementary material at http://dx.doi.org/10.1063/1.3657439 for details of amorphous sample generation and oxide/InGaAs DFT-MD annealing.
[17]G. Gutierrez and B. Johansson, Phys. Rev. B **65**, 104202 (2002).
[18]P. Lamparter and R. Kniep, Physica B **234-236**, 405 (1997).
[19]H. Momida, T. Hamada, and Y. Takagi, Phys. Rev. B **73**, 054108 (2006).
[20]X. Zhao, D. Ceresoli, and D. Vanderbilt, Phys. Rev. B **71**, 085107 (2005).
[21]D. Vanderbilt, X. Zhao, and D. Ceresoli, Thin Solid Films **486**, 125 (2005).
[22]D. Ceresoli and D. Vanderbilt, Phys. Rev. B **74**, 125108 (2006).
[23]V. Gritsenko, D. Gritsenko, S. Shaimeev, V. Aliev, K. Nasyrov, S. Erenburg, V. Tapilin, H. Wong, M. C. Poon, J. H. Lee, J. W. Lee, and C. W. Kim, Microelectron. Eng. **81**, 524 (2005).
[24]A. V. Shaposhnikov, D. V. Gritsenko, I. P. Petrenko, O. P. Pchelyakov, V. A. Gritsenko, S. B. Erenburg, N. V. Bausk, A. M. Badalyan, Yu. V. Shubin, T. P. Smirnova, H. Wong, and C. W. Kim, J. Exp. Theor. Phys. **102**, 799 (2006).
[25]P. Schelling, S. Phillpot, and D. Wolf, J. Am. Ceram. Soc. **84**(7), 1609 (2001).
[26]P. Broqvist and A. Pasquarello, Appl. Phys. Lett. **90**, 082907 (2007).
[27]J.-P. Crocombette and D. Ghaleb, J. Nucl. Mater. **257**, 282 (1998).
[28]H. Takeuchi, D. Ha, and T.-J. King, J. Vac. Sci. Technol. A **22**, 1337 (2004).
[29]V. Gritsenkoa, D. Gritsenkoa, S. Shaimeeva, V. Alieva, K. Nasyrova, S. Erenburgb, V. Tapilinc, H. Wongd, M. C. Poone, J. H. Leef, J.-W. Leef, and C. W. Kimf, Microelectron. Eng. **81**, 524 (2005).
[30]T. V. Perevalov, V. A. Gritsenko, S. B. Erenburg, A. M. Badalyan, H. Wong, and C. W. Kim, J. Appl. Phys. **101**, 053704 (2007).
[31]R. W. Godby, M. Schlüter, and L. J. Sham, Phys. Rev. B **37**, 10159 (1988).
[32]S. Sayan, R. A. Bartynski, X. Zhao, E. P. Gusev, D. Vanderbilt, M. Croft, M. Banaszak-Holl, and E. Garfunkel, Phys. Status Solidi B **241**, 2246 (2004).
[33]E. Bersch, S. Rangan, R. A. Bartynski, E. Garfunkel, and E. Vescovo, Phys. Rev. B **78**, 085114 (2008).
[34]R. Puthenkovilakam and J. P. Chang, Appl. Phys. Lett. **84**, 1353 (2004); S. Miyazaki, J. Vac. Sci. Technol. B **19**, 2212 (2001).
[35]T. Ito, M. Maeda, K. Nakamura, H. Kato, and Y. Ohki, J. Appl. Phys. **97**, 054104 (2005).
[36]M. C. Cheynet, S. Pokrant, F. D. Tichelaar, and J.-L. Rouviere, J. Appl. Phys. **101**, 054101 (2007).
[37]J. Shen, J. B. Clemens, E. Chagarov, D. L. Feldwinn, W. Melitz, T. Song, S. R. Bishop, A. C. Kummel, and R. Droopad, Surf. Sci. **604**, 1757 (2010).
[38]K. Shiraishi, J. Phys. Soc. Jpn. **59**, 3455 (1990).
[39]G. Goryl, D. Toton, M. Goryl, N. Tomaszewska, and J. J. Kolodziej, Surf. Sci. **605**, 2073 (2011).
[40]C. Kumpf, L. D. Marks, D. Ellis, D. Smilgies, E. Landemark, M. Nielsen, R. Feidenhans, J. Zegenhagen, O. Bunk, J. H. Zeysing, Y. Su, and R. L. Johnson, Phys. Rev. Lett. **86**, 3586 (2001).
[41]S. J. Plimpton, J. Comput. Phys. **117**, 1 (1995); see http://lammps.sandia.gov/index.html for information about LAMMPS code.
[42]M. Matsui, Miner. Mag. **58A**, 571 (1994).
[43]G. Kresse and J. Furthmüller, Comput. Mater. Sci. **6**, 15 (1996).
[44]G. Kresse and J. Furthmüller, Phys. Rev. B **54**, 11169 (1996).
[45]P. E. Blöchl, Phys. Rev. B **50**, 17953 (1994).
[46]G. Kresse and J. Joubert, Phys. Rev. B **59**, 1758 (1999).
[47]J. P. Perdew, K. Burke, and M. Ernzerhof, Phys. Rev. Lett. **77**, 3865 (1996).
[48]J. P. Perdew, K. Burke, and M. Ernzerhof, Phys. Rev. Lett. **78**, 1396 (1997).
[49]J. Neugebauer and M. Scheffler, Phys. Rev. B **46**, 16067 (1992).
[50]Y. Hwang, R. Engel-Herbert, and S. Stemmer, Appl. Phys. Lett. **98**, 052911 (2011).
[51]G. Henkelman, A. Arnaldsson, and H. Jonsson, Comput. Mater. Sci. **36**, 354 (2006).
[52]E. Sanville, S. Kenny, R. Smith, and G. Henkelman, J. Comput. Chem. **28**, 899 (2007).
[53]E. Chagarov and A. Kummel (unpublished).
[54]S. J. Clark, L. Lin, and J. Robertson, Microelectron. Eng. **88**, 1464 (2011).
[55]W. Wang, C. L. Hinkle, E. M. Vogel, K. Cho, and R. M. Wallace, Microelectron. Eng. **88**, 1061 (2011).
[56]J. Robertson and L. Lin, in *Proceedings of the 2010 IEEE International Electron Devices Meeting (IEDM)*, San Francisco, CA, pp. 32.6.1−32.6.4, (2010) (IEEE Publishing, New York).
[57]J. Robertson and L. Lin, Microelectron. Eng. **88**, 1440 (2011).
[58]M. Passlack, R. Droopad, Z. Yu, N. Medendorp, D. Braddock, X. W. Wang, T. P. Ma, and T. Büyüklimanli, IEEE Electron. Dev. Lett. **29**, 1181 (2008).
[59]M. Passlack, R. Droopad, and G. Brammertz, IEEE Trans. Electron. Dev **57**, 2944 (2010).
[60]M. Passlack, Z. Yu, R. Droopad, B. Bowers, C. Overgaard, J. Abrokwah, and A. C. Kummel, J. Vac. Sci. Technol. B **17**, 49 (1999).
[61]M. J. Hale, S. I. Yi, J. Z. Sexton, A. C. Kummel, and M. Passlack, J. Chem. Phys. **119**, 6719 (2003).
[62]W. Priyantha, G. Radhakrishnan, R. Droopad, and M. Passlack, J. Crystal Growth **323**, 103 (2011).
[63]C. L. Hinkle, M. Milojevic, B. Brennan, A. M. Sonnet, F. S. Aguirre-Tostado, G. J. Hughes, E. M. Vogel, and R. M. Wallace, Appl. Phys. Lett. **94**, 162101 (2009).
[64]C. L. Hinkle, M. Milojevic, A. M. Sonnet, H. C. Kim, J. Kim, E. M. Vogel, and R. M. Wallace, ECS Trans. **19**, 387 (2009).
[65]D. L. Winn, M. J. Hale, T. J. Grassman, J. Z. Sexton, and A. C. Kummel, J. Chem. Phys. **127**, 134705 (2007).
[66]M. Milojevic, F. S. Aguirre-Tostado, C. L. Hinkle, H. C. Kim, E. M. Vogel, J. Kim, and R. M. Wallace, Appl. Phys. Lett. **93**, 202902 (2008).
[67]F. S. Aguirre-Tostado, M. Milojevic, B. Lee, J. Kim, and R. M. Wallace, Appl. Phys. Lett. **93**, 172907 (2008).

[68]F. S. Aguirre-Tostado, M. Milojevic, C. L. Hinkle, E. M. Vogel, R. M. Wallace, S. McDonnell, and G. J. Hughes, Appl. Phys. Lett. **92**, 171906 (2008).
[69]A. P. Kirk, M. Milojevic, J. Kim, and R. M. Wallace, Appl. Phys. Lett. **96**, 202905 (2010).
[70]H. D. Trinh, E. Y. Chang, P. W. Wu, Y. Y. Wong, C. T. Chang, Y. F. Hsieh, C. C. Yu, H. Q. Nguyen, Y. C. Lin, K. L. Lin, and M. K. Hudait, Appl. Phys. Lett. **97**, 042903 (2010).
[71]B. Shin, J. B. Clemens, M. A. Kelly, A. C. Kummel, and P. C. McIntyre, Appl. Phys. Lett. **96**, 252907 (2010).
[72]E. J. Kim, E. Chagarov, J. Cagnon, Y. Yuan, A. C. Kummel, P. M. Asbeck, S. Stemmer, K. C. Saraswat, and P. C. McIntyre, J. Appl. Phys. **106**, 124508 (2009).
[73]B. Shin, D. Choi, J. S. Harris, and P. C. McIntyre, Appl. Phys. Lett. **93**, 052911 (2008).
[74]P. C. McIntyre, Y. Oshima, E. Kim, E. Chagarov, J. Cagnon, K. C. Saraswat, S. Stemmer, and A. C. Kummel, in *Proceeding of the Semiconductor Interface Specialists Conference (SISC)*, San Diego, CA, 2008, p. 133 (IEEE Publishing, New York)..
[75]P. C. McIntyre, Y. Oshima, E. Kim, and K. C. Saraswat, Microelectron. Eng. **86**, 1536 (2009).
[76]J. B. Clemens, E. A. Chagarov, M. Holland, R. Droopad, J. Shen, and A. C. Kummel, J. Chem. Phys. **133**, 154704 (2010).
[77]W. Melitz, T. Kent, J. Shen, and A. C. Kummel, Surface cleaning and monolayer seeding for ALD of high-k studied by in situ STM, STS, and XPS, in *Proceedings of the AVS 2011*, Nashville, TN, 2011 (American Institute of Physics, New York).
[78]Y. H. Chang, M. L. Huang, P. Chang, C. A. Lin, Y. J. Chu, B. R. Chen, C. L. Hsu, J. Kwo, T. W. Pi, and M. Hong, Microelectron. Eng. **88**, 440 (2011).
[79]J. R. Weber, A. Janotti, and C. G. Van de Walle, Microelectron. Eng. **86**, 1756 (2009).
[80]J. Huang, N. Goel, H. Zhao, C. Y. Kang, K. S. Min, G. Bersuker, S. Oktyabrsky, S. Koveshnikov, J. C. Lee, P. Majhi, W. Tsai, P. D. Kirsch, H.-H. Tseng, and R. Jammy, in *Proceedings of the International Electron Device Meeting (IEDM)*, Baltimore, MD, 2009, p. 13.5 (IEEE Publishing, New York).
[81]Y. Xuan, T. Shen, Y. Q. Wu, M. Xu, and P. D. Ye, in *Proceedings of the 66th Annual Device Research Conference (DRC)*, Santa Barbara, CA, 2008, pp. 37−38 (IEEE Publishing, New York).
[82]Y. Xuan, T. Shen, M. Xu, Y. Q. Wu, and P. D. Ye, in *Proceedings of the IEDM*, San Francisco, CA, 2008, p. 371 (IEEE Publishing, New York).
[83]Y. Xuan, Y. Q. Wu, and P. D. Ye, IEEE Electron Device Lett. **29**, 294 (2008).
[84]M. Egard, L. Ohlsson, B. M. Borg, L.-E. Wernersson, and E. Lind, in *Proceedings of the Abstracts of the IEEE Device Research Conference 2011*, Santa Barbara, CA, 28 June 2011 (IEEE Publishing, New York).
[85]J. Robertson, Microelectron. Eng. **86**, 1558 (2009).
[86]J. Robertson, Appl. Phys. Lett. **94**, 152104 (2009).
[87]P. D. Ye, Y. Xuan, Y. Q. Wu, and M. Xu, ECS Trans. **19**, 605 (2009).
[88]U. Singisetti, M. A. Wistey, G. J. Burek, A. K. Baraskar, J. Cagnon, B. Thibeault, A. C. Gossard, S. Stemmer, M. J. W. Rodwell, E. Kim, B. Shin, P. C. McIntyre, and Y.-J. Lee, in *Proceedings of the IPRM'09*, Newport Beach, CA, 2009, p. 120 (IEEE Publishing, New York).
[89]M. Caymax, G. Brammertz, A. Delabie, S. Sioncke, D. Lin, M. Scarrozza, G. Pourtois, W.-E. Wang, M. Meuris, and M. Heyns, Microelectron. Eng. **86**, 1529 (2009).
[90]H. Zhao, Y.-T. Yen-Ting Chen, J. H. Yum, Y. Wang, N. Goel, and J. C. Lee, Appl. Phys. Lett. **94**, 193502 (2009).
[91]S. J. Bentley, M. Holland, L. Xu, G. W. Paterson, Z. Haiping, O. Ignatova, D. Macintyre, S. Thoms, A. Asenov, S. Byungha, A. Jaesoo, P. C. McIntyre, and I. G. Thayne, IEEE Electron Dev. Lett. **32**, 494 (2001).
[92]M. Radosavljevic, B. Chu-Kung, S. Corcoran, G. Dewey, M. K. Hudait, J. M. Fastenau, J. Kavalieros, W. K. Liu, D. Lubyshev, M. Metz, K. Millard, N. Mukherjee, W. Rachmady, U. Shah, and R. Chau, in *Proceedings of the 2009 IEEE International Electron Devices Meeting (IEDM)*, Baltimore, MD, 2009, pp. 1–4 (IEEE Publishing, New York).
[93]M. Radosavljevic, G. Dewey, J. M. Fastenau, J. Kavalieros, R. Kotlyar, B. Chu-Kung, W. K. Liu, D. Lubyshev, M. Metz, K. Millard, N. Mukherjee, L. Pan, R. Pillarisetty, W. Rachmady, U. Shah, and R. Chau, in *Proceedings of the 2010 IEEE International Electron Devices Meeting (IEDM)*, San Francisco, CA, 2010, pp. 6.1.1−6.1.4 (IEEE Publishing, New York).
[94]R. Suri, D. J. Lichtenwalner, and V. Misra, Appl. Phys. Lett. **96**, 112905 (2010).
[95]Y. C. Chang, M. L. Huang, K. Y. Lee, Y. J. Lee, T. D. Lin, M. Hong, J. Kwo, T. S. Lay, C. C. Liao, and K. Y. Cheng, Appl. Phys. Lett. **92**, 072901 (2008).
[96]M. L. Huang, Y. C. Chang, Y. H. Chang, T. D. Lin, J. Kwo, and M. Hong, Appl. Phys. Lett. **94**, 052106 (2009).
[97]T. D. Lin, P. Chang, H. C. Chiu, Y. C. Chang, C. A. Lin, W. H. Chang, Y. J. Lee, Y. H. Chang, M. L. Huang, J. Kwo, and M. Hong, in *Proceedings of the 2009 IEEE International Conference on Indium Phosphide and Related Materials*, Newport Beach, CA, 2009, p. 94 (IEEE Publishing, New York).
[98]D. C. Suh, Y. D. Cho, D.-H. Ko, K. B. Chung, M.-H. Cho, and Y. Lee, ECS Trans. **19**, 233 (2009).
[99]Y. Hwang, R. Engel-Herbert, N. G. Rudawski, and S. Stemmer, J. Appl. Phys. **108**, 034111 (2010).
[100]S. Oktyabrsky, V. Tokranov, S. Koveshnikov, M. Yakimov, R. Kambhampati, H. Bakhru, R. Moore, and W. Tsai, J. Cryst. Growth **311**, 1950 (2009).
[101]J. B. Clemens, S. R. Bishop, J. S. Lee, A. C. Kummel, and R. Droopad, J. Chem. Phys. **132**, 244701 (2010).
[102]P. Chang, W. C. Lee, M. L. Huang, Y. J. Lee, M. Hong, and J. Kwo, J. Vac. Sci. Technol. B **28**, C3A9 (2010).
[103]Y. Q. Wu, M. Xu, Y. Xuan, P. D. Ye, J. Li, Z. Cheng, and A. Lochtefeld, in *Proceedings of the 17th Biennial UGIM 2008*, 2008, pp. 49–52 (IEEE Publishing, New York).
[104]S. Koveshnikov, N. Goel, P. Majhi, H. Wen, M. B. Santos, S. Oktyabrsky, V. Tokranov, R. Kambhampati, R. Moore, F. Zhu, J. Lee, and W. Tsai, Appl. Phys. Lett. **92**, 222904 (2008).
[105]S. Koveshnikov, N. Goel, P. Majhi, C. K. Gaspe, M. B. Santos, S. Oktyabrsky, V. Tokranov, M. Yakimov, R. Kambhampati, H. Bakhru, F. Zhu, J. Lee, and W. Tsai, in *Proceedings of the 66th Annual Device Research Conference (DRC)*, Santa Barbara, CA, 2008, pp. 43−44 (IEEE Publishing, New York).
[106]S. Stemmer, in *Proceedings of the 2009 VLSI Technology Conference*, Kyoto, Japan, 2009 (IEEE Publishing, New York).